

High-temperature EPR in solid and molten paramagnets*

E. Dormann,[†] D. Hone, and V. Jaccarino

Department of Physics, University of California, Santa Barbara, California 93106

(Received 19 January 1976)

The electron-paramagnetic-resonance (EPR) linewidth ΔH of the strongly exchange coupled paramagnets, MnF_2 , KMnF_3 , RbMnF_3 , and CsMnF_3 , was studied from 300 to 1450 K. Relative to the Néel temperature T_N this region encompasses temperatures of the order of $3 < T/T_N < 15$ in the solid and some 200–350°K into the molten state. The XMnF_3 ($X = \text{K}, \text{Rb}, \text{and Cs}$) salts all show a ΔH which monotonically increases with temperature up to the melting point T_m . At T_m an abrupt doubling of ΔH occurs, followed by a decreasing linewidth with increasing temperature. The linewidth of MnF_2 exhibits a most striking behavior; beginning some 200°C below T_m the linewidths ΔH^{\parallel} and ΔH^{\perp} (parallel or perpendicular to c axis) decrease rapidly, with the anisotropy $(1 - \Delta H^{\parallel} / \Delta H^{\perp})$ in ΔH changing sign before melting. No abrupt change in ΔH is found upon melting. EPR in magnetically diluted but structurally isomorphic salts (e.g., $\text{KMn}_{1-x}\text{Mg}_x\text{F}_3$) was investigated in both solid and molten states. Resolved ^{55}Mn and ^{19}F hfs were found in the very dilute solids but not in the liquids. Linewidths as functions of concentration were obtained in both cases. A theoretical interpretation of the temperature dependence of ΔH in the dense magnetic salts is given. Rigid-lattice spin dynamical contributions are examined and are found to be small. Lattice vibrational effects (harmonic and anharmonic) on the temperature dependence of the dipolar and exchange interactions, as they affect the linewidth, were studied. From the combined theoretical and experimental studies, for the simple cubic KMnF_3 and RbMnF_3 compounds, the temperature dependence of the exchange interaction is deduced in the region $T = 4T_N$ to $T = T_m$. The anomalous behavior of the MnF_2 linewidth and its anisotropy below T_m is interpreted as resulting from the activated interchange of nearest-neighbor Mn^{2+} ions along the c axis, with $E_0 \approx 0.3$ eV. The magnitudes of the linewidth in the molten states of all of the dense paramagnets are shown to correspond to a correlation time for spin exchange or motion (and/or chemical exchange) $\tau_m \approx 10^{-12}$ sec. The dilution experiments in the molten state suggest that spin exchange continues to be important in the liquid until very low magnetic ion concentrations.

I. INTRODUCTION

The structure and width of electron-paramagnetic-resonance (EPR) and nuclear-magnetic-resonance (NMR) line profiles yield information on the amplitude and spectral density of the local-field fluctuations from which certain characteristic properties of the electronic-spin-correlation functions may be inferred. Such information for the high-temperature solid and molten phase of paramagnets is scarce. EPR studies of the molten state have been confined mainly to diluted chlorides,¹⁻³ where the question of observability or narrowing of the ^{55}Mn hyperfine structure (hfs) was of primary interest.

We began our investigations with the intent of understanding high-temperature "motion" in the broadest sense—including the influence of lattice vibrations in the solid as well as atomic migration. The fluoride salts of manganese were chosen—despite their chemical aggressivity at high temperatures—because the S -like character of the Mn^{2+} free-ion ground state simplifies the interpretation considerably and because dipolar, ^{55}Mn hyperfine, as well as ^{19}F superhyperfine, interactions can be studied. Specifically, we examined (cubic) KMnF_3 and RbMnF_3 , (hexagonal) CsMnF_3 , and (tetragonal) MnF_2 . In addition, a parallel

study of the ^{19}F NMR in these same substances was conducted in our laboratory⁴ in the hope of obtaining complementary information.

After providing the details of the experimental procedures in Sec. II, we give the EPR linewidth results for the solid and molten states of the above-mentioned *pure* materials in Sec. III. In addition, the results obtained on *mixed* magnetic fluorides (e.g., KMnF_3 - MnF_2) in the molten state as well as magnetically diluted systems, in both solid and molten states, are given in the same section.

In Sec. IV, an interpretation of the experimental results is presented. We first note that rigid-lattice theories, as developed in the Appendix, are qualitatively inadequate to explain the observed temperature dependence of ΔH . (The Appendix examines two such theories in some detail; the first utilizes the relaxation function approach of Mori and Kawasaki⁵ as applied to the EPR linewidth problem by Mori⁶ and by Huber.⁷ The second is the dynamical Green's-function theory of Tomita and Tanaka.⁸⁻¹⁰) A simple theory of lattice vibrational effects (both harmonic and anharmonic) on the dipolar and exchange interactions is given and the temperature dependence of these quantities and the linewidth is estimated for KMnF_3 and RbMnF_3 . For these two com-

pounds the spin dynamical and lattice vibrational theoretical results and the experimental measurements are combined to obtain the temperature dependence of the exchange interaction in the region $4T_n < T < T_m$. For MnF_2 the anomalous behavior of the linewidth just below T_m is interpreted in terms of an activated *interchange* of near-neighbor Mn ions along the crystal *c* axis with $E_a \approx 0.3$ eV. Finally, a qualitative discussion of the molten-state results is presented showing that the time that characterizes the decay of the relevant correlation function, whether due to spin exchange and/or motion, is of the order $\tau_m \approx 10^{-12}$ sec in all of the dense paramagnets.

II. EXPERIMENTAL PROCEDURES

The samples utilized in this investigation were prepared in the Solid-State Materials Laboratory of the University of California, Santa Barbara Physics Dept. The starting material for the crystal preparation was obtained by precipitation using analytical reagent-grade chemicals. For example, RbMnF_3 was formed by adding MnCO_3 to a solution containing a slight excess of RbF in 48-volume% HF acid. The main source of transition-metal-ion impurities for the crystals was the fact that the MnCO_3 contained about 500-ppm Zn and ≤ 10 -ppm Fe or Ni. These in no way affected our linewidth measurements.

All EPR measurements were made at about 9.3 GHz with a simple "magic tee" microwave bridge. Figure 1 gives a sketch of the setup. An Impatt diode was used as a constant-frequency rf source.¹¹ Of particular advantage was the low noise of the Impatt diode near the carrier frequency, when using low-frequency magnetic field modulation as required by the construction of our cavity. The extreme simplicity of the setup lent itself to easy adjustments in the frequency mode when samples melted, and provided longtime frequency stability. For most measurements, the relatively low maximum power level of about 10 mW and the poor sensitivity of 2×10^{14} spins/Oe of width at ambient temperature with a 1-sec time constant, was adequate. In any case, the main difficulty in the molten-state experiments was frequency and amplitude modulation noise resulting from the bubbling of the liquids.

In addition, a frequency-modulated klystron, connected via a 20-dB cross coupler, was used to "set up" the measurements; e.g., to adjust the hole and screw-type coupling of the cavity, to determine the temperature dependence of the cavity's loaded Q , or to allow tuning of the Impatt diode (variable but unmodulated in frequency) unambiguously to the cavity resonance and not ac-

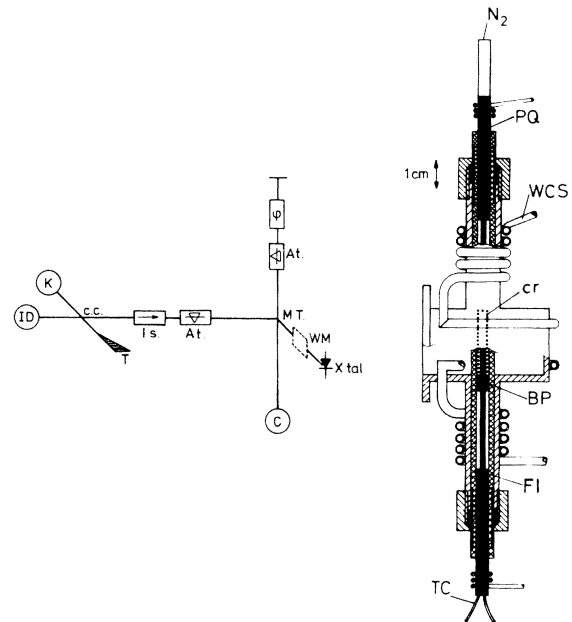


FIG. 1. Sketch of microwave setup (left) and high-temperature TE_{102} cavity (right). Left: ID: Impatt diode; K: klystron; T: $50\text{-}\Omega$ termination; cc: 20-dB cross coupler; Is: isolator; At: attenuator; MT: magic tee; ϕ : phase shifter; C: cavity; WM: wavemeter; Xtal: crystal detector. Right: PQ: platinum-pasted sand-blasted quartz heater tube with soft-soldered contacts; FI: Fiberfrax insulation; BP: boron nitride plug, place of thermocouple; TC: thermocouple feedthrough; cr: crucible made of pyrolytic boron nitride (oriented for higher thermal conductivity parallel to long axis) with sample and boron nitride plug. Sample size and position (filling factor) varied in order to fulfill the conditions of sufficient number of spins, no radiation broadening and $d > \delta$ (see text), N_2 : connection to nitrogen; WCS: water-cooling system.

cidental to some spurious power minimum.

Fiberfrax insulation of platinum-strip-coated sandblasted quartz tubes allowed our water-cooled TE_{102} cavity of the Singer *et al.*¹² type to be operated up to temperatures of about 1400°C . Sample containment and/or decomposition (oxidation) ultimately limited how high in temperature a given experiment could be performed. The thickness of the resistance-heated Pt strips was adjusted so as to minimize temperature gradients inside the cavity. Strips with constant cross section led to large temperature differences between the sample center and a point 3 mm below the bottom of the cavity (where the thermocouple was placed during EPR measurements). However, the resistance in the center region of the heater could be decreased by trial and error (e.g., painting more Pt paste in this region) so as to reduce temperature differences over the designated length

to $\pm 10^\circ\text{C}$ up to 1100°C .

Most temperature measurements were performed with chromel-alumel thermocouples. With our well-filtered current or voltage controlled dc power supply, temperature stability during measurement exceeded $\pm 1^\circ\text{C}$. Hence the error bars shown in the following figures give the uncertainty in *absolute* value of the temperature. As is common practice in high-temperature physical chemistry we use the centigrade scale for the experimental results.

Because of the extremely corrosive properties of the fluoride salts at high temperatures (particularly when they are molten) it was necessary to contain them in crucibles made of pyrolytic boron nitride,¹³ closed with a plug of sintered boron nitride. Closed crucibles were essential to prevent oxidation and decomposition despite the fact that precaution was taken to surround the heater tube with dry N_2 . The noncubic samples could easily be oriented by x rays and optical means to better than 1° . However, upon transferring into the crucible and then into the cavity, alignment with respect to the magnetic field was often not better than $\pm 3.5^\circ$. This could be inferred from measurements of the angular dependence of the linewidth.

In all of the systems studied, the lines in both the magnetically *dense* solid and molten paramagnets were Lorentzian in shape, to within experimental accuracy. The peak-to-peak linewidth (ΔH_{pp}) in the solid state was determined from a comparison of the theoretical with the observed derivatives of absorption lines, recorded using 280-Hz field modulation.¹⁴ Especially in the lower-temperature range where the volume susceptibility is large, care had to be taken to prevent radiation-induced broadening due to inadmissibly large sample size.¹⁵ An additional problem with the molten salts is that they have an appreciable electrical conductivity [e.g., $\sigma \approx 5$ ($\Omega\text{ cm}$)⁻¹ and a skin depth δ of about $\frac{1}{4}$ mm for MnF_2 at 9.3 GHz and 1000°C]. Therefore, in order to observe well-defined line shapes, a sample size $d \gg \delta$ or $d \ll \delta$ must be used.¹⁶

Large samples were used to try to realize the first extreme. Alternatively, two procedures were employed, both of which gave identical values of ΔH_{pp} to within experimental error; either (a) the bridge was tuned for absorption but combined absorption-dispersion signals were observed. As is well known in EPR in metals the recorded lines can then be analyzed using the diagrams given by Peter *et al.*,¹⁷ or (b) the bridge was adjusted by trial and error with varying mixtures of absorption and dispersion until a simple absorption derivative line profile was obtained.

This was then analyzed as it would be in the solid state.

The use of "large" samples—unfavorable only for the very dilute systems—gave us convenient access to supplementary information; for example, we could observe and follow semiquantitatively how samples became conductive via their microwave losses well below T_m (e.g., MnF_2 begins to be noticeably conductive well below T_m), and a decrease in the asymmetry in the line profile in the molten state signaled the onset of increasing sample oxidation. Since oxides of Mn with higher melting temperatures yield linewidths that are similar in many instances to the ones reported here, temperature reversibility of the measurements played a crucial role. For these reasons it was essential to take polycrystal as well as single-crystal data in the solid state.

III. EXPERIMENTAL RESULTS

A. Solid-state pure systems

1. $X\text{MnF}_3$ ($X = \text{Rb}, \text{K}, \text{Cs}$)

The EPR linewidth ΔH has been investigated by others in the temperature region *below* 300 K. Their results may be briefly characterized as follows: In RbMnF_3 ,¹⁸ ΔH is virtually constant with some slight narrowing as T approaches $T_N = 83$ K; KMnF_3 is reported to have a temperature independent ΔH ,¹⁹ even near $T_N = 88$ K, while hexagonal CsMnF_3 exhibits a characteristic critical divergence of ΔH as T approaches $T_N = 55.3$ K.²⁰

Our measurements, which begin at 300 K and are shown in Figs. 2 and 3, reveal a somewhat similar behavior for all three $X\text{MnF}_3$ compounds with regard to the temperature dependence of ΔH . In a rough fashion, we may characterize the linewidths as showing an approximately linear in-

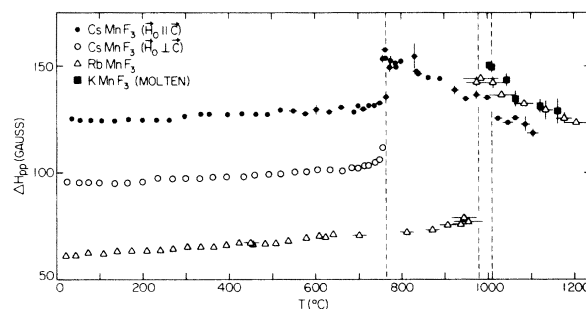


FIG. 2. Temperature dependence of the EPR linewidth for the solid and molten double fluorides KMnF_3 , RbMnF_3 , and CsMnF_3 . The solid-state data of KMnF_3 are not included but are given separately in Fig. 3, because of the extreme similarity to the RbMnF_3 data. The broken vertical lines indicate the respective melting points.

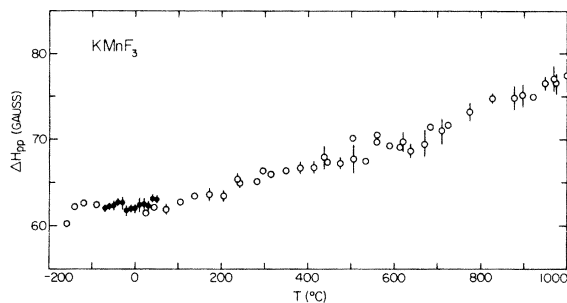


FIG. 3. Temperature dependence of the linewidth for solid KMnF_3 at 9.3 GHz. The solid circles represent averages over at least three measurements. Accuracy of the data below 25°C is poor, because we used our high-temperature cavity system for these measurements.

crease in ΔH with T that persists until the vicinity of the melting point T_m , with the following values of $\delta\Delta H/\delta T$: 14.3 ± 1.6 (RbMnF_3), 13.8 ± 0.9 (KMnF_3), and 9.5 ± 1.8 ($\vec{H}_0 \parallel \vec{c}$; CsMnF_3), 11.3 ± 1.3 ($\vec{H}_0 \perp \vec{c}$; CsMnF_3), all in units of mGs/K. Although we will defer until Sec. IV a discussion of the various spin and lattice dynamical effects that may contribute to the variation of ΔH with T , it is worth noting here that a variation of 15% in ΔH for RbMnF_3 between 300 K and T_m , for example, is clearly a non-negligible effect.

2. MnF_2

Again, the EPR linewidth has been studied extensively,²¹ between 380 K and $T_N = 67.3$ K, by a

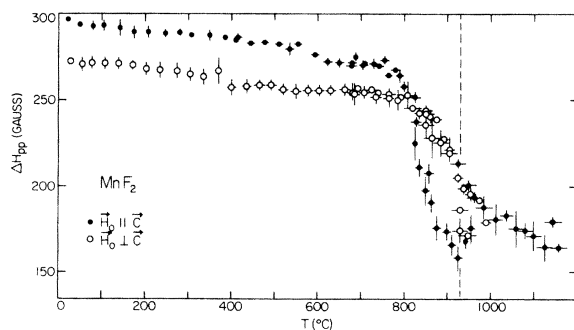


FIG. 4. Temperature dependence of the linewidth of oriented single crystals of MnF_2 . The broken vertical line indicates the melting point. The range 700–1000°C was measured twice for both orientations. The scatter of the data just above the melting point shows the problems that the poor thermal conductivity of the samples creates in this region. It can be seen that one sample with $\vec{H}_0 \perp \vec{c}$ lost its orientation at the melting point and that usually at least one point "above T_m " could be recorded where still part of the oriented crystal was left. The linewidth of molten MnF_2 at 930°C is about 205 G. (See also Fig. 8.) For the true molten-state data of MnF_2 given as solid circles too, the melting point was approached from the high-temperature side.

variety of workers. Particular attention has been given to both the critical divergence of ΔH as T approaches T_N and the anisotropic behavior of ΔH in this body-centered-tetragonal spin system.^{22, 23}

Our high-temperature measurements, extending from 300 K to the melting point $T_m = 1200$ K, are shown in Fig. 4. In contrast to the increase of ΔH with T that was found for all three of the XMnF_3 compounds, an even stronger nonlinear decrease of the EPR linewidth with increasing T is seen in MnF_2 . Up to about 600°C the ratio $\Delta H(\parallel c)/\Delta H(\perp c)$ remains constant with a value 1.081 ± 0.008 .

Perhaps the most striking feature of the MnF_2 -linewidth temperature dependence is that, beginning more than 200° below T_m , ΔH decreases even more rapidly and the anisotropy in the linewidth $[1 - \Delta H(\parallel c)/\Delta H(\perp c)]$ actually changes sign! This effect, which appears to be a precursor to melting, is accompanied by a marked increase in the microwave conductivity (and losses). Both the latter effect and the lack of an abrupt change in ΔH at T_m seem to be peculiar to MnF_2 .²⁴

B. Solid-state dilute systems

The impure paramagnet was also investigated as a function both of impurity concentration and of temperature. The results on substitutional magnetic impurities (Fe^{2+} or Co^{2+}) for the Mn^{2+} in KMnF_3 will be reported elsewhere—these complement and extend the work of Gulley and Jaccarino²⁵ at lower temperatures. Here we confine our attention to the effects of dilution—specifically the effects of substituting nonmagnetic Mg^{2+} or Zn^{2+} for the Mn^{2+} in KMnF_3 . The motivation was primarily one of determining the temperature dependence of the ^{55}Mn and ^{19}F hyperfine parameters in the magnetically dilute systems but we were also interested in the concentration dependence of the EPR line profile. Since the spectra of the magnetically dilute noncubic systems are considerably more complex and anisotropic,²⁶ we have deliberately avoided studies of, say, $\text{Mn}_x\text{Zn}_{1-x}\text{F}_2$.

1. Concentration dependence of the line profile and width

$\text{KMn}_x(\text{Mg}, \text{Zn})_{1-x}\text{F}_3$: A series of measurements of the line profile and width was carried out at 300 K for the systems $\text{KMn}_x\text{Mg}_{1-x}\text{F}_3$ and $\text{KMn}_x\text{Zn}_{1-x}\text{F}_3$, as functions of concentration x . Most of the measurements were made on cubic $\text{KMn}_x\text{Mg}_{1-x}\text{F}_3$, although essentially identical results were obtained on the $\text{KMn}_x\text{Zn}_{1-x}\text{F}_3$ samples, if the latter were stabilized in the cubic form from the melt.²⁷

First, with regard to the actual line profile, we show in Fig. 5 the derivative of the EPR line as a function of field for various concentrations $1 - x$

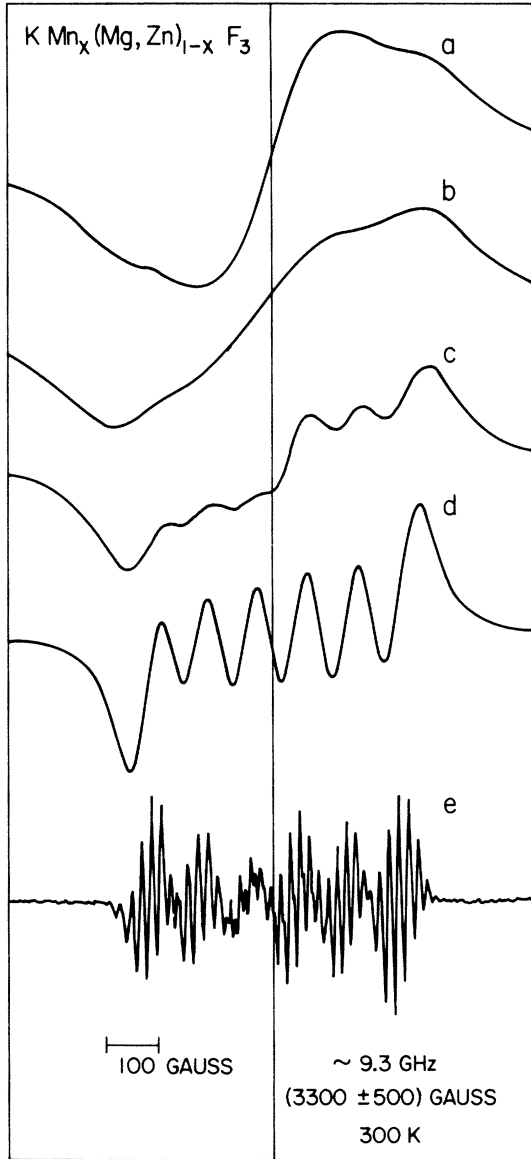


FIG. 5. Derivative EPR line shapes that show the appearance of ^{55}Mn hyperfine structure and ^{19}F super-hyperfine structure in $\text{KMn}_x(\text{Mg}, \text{Zn})_{1-x}\text{F}_3$ at 300 °K. Nominal concentrations: (a) and (c): $\text{KMn}_x\text{Zn}_{1-x}\text{F}_3$ with $x \geq 0.10$ and $x = 0.04$; (b), (d), and (e): $\text{KMn}_x\text{Mg}_{1-x}\text{F}_3$ with $x \leq 0.10$, 0.01, and 0.001.

of Mg or Zn (see Fig. 5 caption). Recalling the fact that for the magnetically pure materials ($x = 1$) the line profile is Lorentzian and unstructured, we see the indications of structure in the resonance appearing first at $x \geq 0.1$. For still smaller concentrations of Mn ($x \approx 0.001$) the full, superimposed, ^{19}F and ^{55}Mn hfs is resolved. Further dilution results only in a diminished intensity. Next, in Fig. 6 we show the concentration depen-

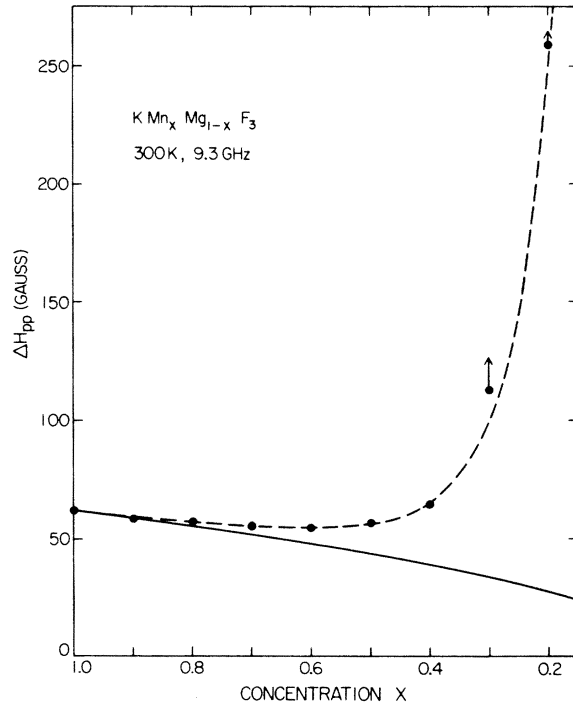


FIG. 6. Concentration dependence of the linewidth for $\text{KMn}_x\text{Mg}_{1-x}\text{F}_3$ at 300 °K. The arrows at the points for low manganese concentration x indicate that here the wings of the recorded lines are broader than those corresponding to a Lorentzian line with the given peak-to-peak width. The solid line gives the x dependence expected for the dipolar broadened exchange narrowed linewidth at higher x ; the broken line through the data is a curve $\Delta H_{pp} = 59.7(x^{1/2} + 0.03x^{-3})\text{G}$.

dence of the linewidth ΔH_{pp} in the system $\text{KMn}_x\text{Mg}_{1-x}\text{F}_3$. For large Mn concentration ($x \geq 0.4$) the line profiles are Lorentzian as far out into the line as one may reasonably examine. Below $x \approx 0.4$ the “wings” of the recorded lines are broader than what would be expected from a Lorentzian line profile, with the given peak-to-peak width indicated by the solid dot. The placement of the arrows is designed to show the direction of the departure from Lorentzian behavior. This is, in part, a forerunner of the actual structure which is subsequently to appear at small x , as we have seen in Fig. 5. The significance of the solid and dashed lines will be discussed later in connection with the interpretation of these experimental results.

2. Temperature dependence of the hyperfine structure (dilute) and EPR widths (dense)

(a) ^{55}Mn and ^{19}F hyperfine parameters in the very dilute limit ($x \approx 0.001$). In the system $\text{KMn}_x\text{Mg}_{1-x}\text{F}_3$, with nominal concentration $x = 0.001$, the temperature dependence of the ^{55}Mn and ^{19}F hyper-

fine parameters (A^{55} and A^{19}) were determined from a standard²⁶ analysis of the spectra such as was displayed in Fig. 5(e). In Fig. 7 we plot the ratios $A^{55}(T)/A^{55}(T_0)$ and $A_s^{19}(T)/A_s^{19}(T_0)$ as functions of temperature up to the melting point ($T_m = 1080^\circ\text{C}$), with $T_0 = 300\text{ K}$. Only the isotropic part of the ^{19}F superhyperfine coupling A_s^{19} is given because powdered samples were used for making the relative variation measurements. The normalizing room-temperature values were obtained by averaging over ten independent measurements. The temperature dependence of $A^{55}(T)/A^{55}(T_0)$ was independently obtained from an analysis of the spectra shown in

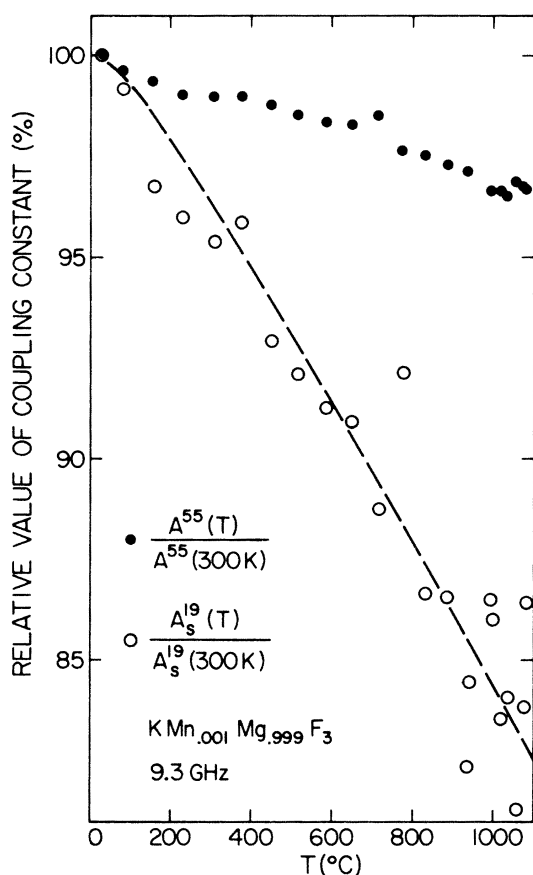


FIG. 7. Temperature dependence of the relative hfs and super-hfs coupling constants $A^{55}(T)/A^{55}(300\text{ K})$ and $A_s^{19}(T)/A_s^{19}(300\text{ K})$, derived from measurements on polycrystalline samples of $\text{KMn}_{0.001}\text{Mg}_{0.999}\text{F}_3$ up to the melting point. The room-temperature values were found as an average over ten independent measurements. $A^{55}(T)$ was calculated from the separation of four peaks in the powder derivative spectra at each T , and $A_s^{19}(T)$ from more than 20. Despite the relatively moderate scatter of the data points, it should be noted that the biggest standard deviations apparent at high-temperature result in an uncertainty of 3.8 and 9.7% for the relative hfs and super-hfs coupling constants. The dashed line is a "best fit" to the data.

Fig. 5(d) where $x = 0.01$. The results so obtained were consistent with those shown in Fig. 7 although the errors were necessarily larger because of the larger widths of the hfs components at the higher concentrations of Mn ions.

(b) ΔH_{pp} vs T in the concentrated limit ($x \geq 0.4$). The broad and complicated line profiles observed at intermediate concentrations $0.4 \geq x \geq 0.01$ preclude a detailed temperature-dependent study for such systems. At $x \geq 0.4$, where again the line profile assumes a Lorentzian shape one might hope to study ΔH vs T as was done for the pure systems. Even in this high-concentration limit we experienced some difficulties in obtaining identical results on two different melts with the same nominal concentrations. We presume this reflects a concentration fluctuation that might be present in any one melt. No detailed plots of the data are given although, as in the dense KMnF_3 , ΔH was observed to increase roughly linearly with T . We were able to estimate the following values for $\delta\Delta H/\delta T$: For $x = 0.9$, 12.8 ± 0.9 (Zn), 12.0 ± 0.9 (Mg); for $x = 0.7$, 11.2 ± 1.0 (Mg), and for $x = 0.5$, 10.1 ± 0.8 (Mg), all in units of mGs/K. Recall that for the pure crystal, $x = 1$, $\delta\Delta H/\delta T = 13.8 \pm 0.9$. See Table I.

C. Molten state

1. Pure systems; XMnF_3 ($X = \text{Rb, K, Cs}$)

The EPR linewidth ΔH through the melting point is shown on the right-hand side of Fig. 2 for the XMnF_3 compounds and in Fig. 4 for MnF_2 . On an expanded scale the molten-state results for MnF_2 (open circles) and KMnF_3 (solid dots) are shown in Fig. 8.

Two regions are to be distinguished in each case: the immediate vicinity of T_m and the behavior well away from the melting point. The XMnF_3 compounds exhibit an abrupt increase in ΔH at T_m in going from solid to molten states. Not surprisingly, perhaps, the magnitude of ΔH at T_m is quite similar for the three compounds. Each exhibits a pronounced decrease of ΔH with T above T_m ,

TABLE I. Variation of the linewidth with temperature in the magnetically diluted crystals $\text{KMn}_x\text{Mg}_{1-x}\text{F}_3$. The significance of the approximate constancy of $(1/\Delta H)(\delta\Delta H/\delta T)$ at large x is discussed in Sec. IV B1.

x	$\frac{\delta\Delta H}{\delta T}$ (10^{-3} G/K)	ΔH (G) at 300 K	$\frac{1}{\Delta H} \frac{\delta\Delta H}{\delta T}$ (10^{-3} /K)
1.0	13.8 ± 0.9	62	0.22
0.9	12.0 ± 0.9	58	0.21
0.7	11.2 ± 1.0	55	0.20
0.5	10.1 ± 0.8	58	0.17

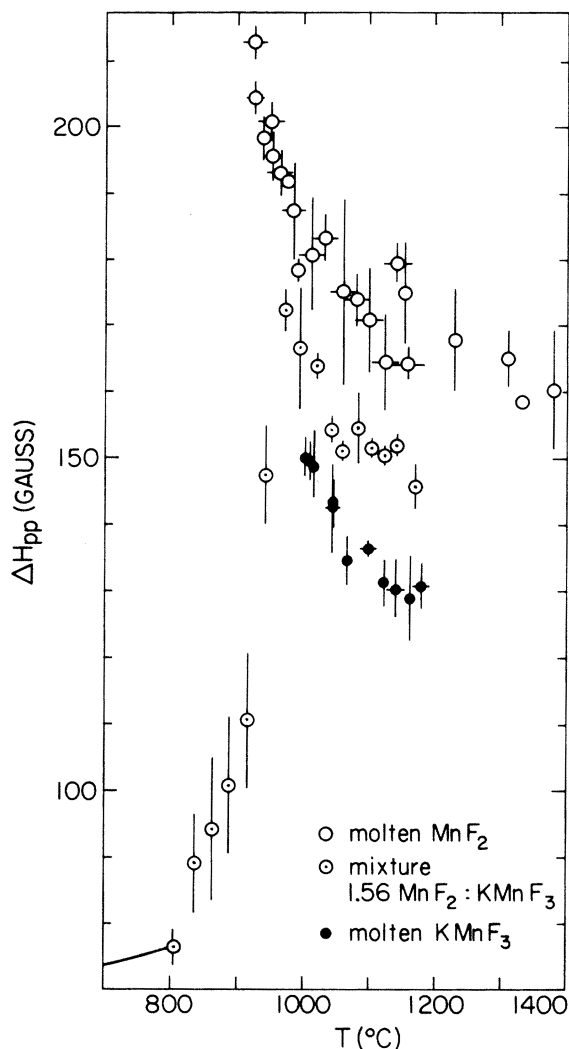


FIG. 8. Comparison of the temperature dependence of the linewidth for molten MnF_2 , molten KMnF_3 , and a mixture 1.56 MnF_2 :1 KMnF_3 . In all cases, the melting point was approached from higher temperatures. For the mixed system, molten, partly molten, and solid regions can be distinguished.

with an initial slope roughly an order of magnitude larger than—and of opposite sign to—the solid-state value. The rate of decrease is noticeably larger at T_m than at higher temperatures; from Figs. 2 and 8 we may estimate $\delta\Delta H/\delta T$ to change from -180 to -50 for KMnF_3 and from -150 to -70 for RbMnF_3 in going from T_m to approximately 1200°C , while $\delta\Delta H/\delta T$ has an average value of -110 (CsMnF_3) in that same range, all in units of mGs/K .

The behavior of ΔH in the immediate vicinity of T_m is noticeably different for MnF_2 . First, it is recalled that in the solid state, as a precursor to melting, both $\Delta H(\parallel c)$ and $\Delta H(\perp c)$ began to decrease

rapidly well below T_m . (See Fig. 4.) The most reliable data at, and above, T_m were obtained by cooling the melt and this is what is shown in Fig. 8. The value of $\Delta H(T_m) = 205.5 \pm 7.5$ G is very close to $\Delta H(\perp c)$ at T_m obtained by melting of the solid. Hence, a discontinuity exists primarily in the change that occurs in going from $\Delta H(\parallel c)$ just below T_m to $\Delta H(T_m)$ in the molten state. Perhaps what is most significant is that $\Delta H(T_m)$ for MnF_2 is definitely larger than $\Delta H(T_m)$ for the three XMnF_3 compounds. Again well above T_m ΔH decreases rapidly with temperature with a slope $\delta\Delta H/\delta T$ varying from -230 at T_m to -40 at temperatures close to 1400°C , in units of mGs/K .

The fact that we were able to make measurements at higher temperatures for MnF_2 than was possible for the XMnF_3 systems was simply a consequence of the rapid loss of alkali fluoride material (decomposition) above 1200°C for the latter.²⁸

2. Mixed, magnetically dense systems (KMnF_3 : MnF_2)

The XMnF_3 and MnF_2 systems are really exceptional melts in that they represent pure or congruently melted compounds. Each system has a well-defined T_m and melting and recrystallization is a completely reversible process with the sole qualification that one may not necessarily obtain a single crystal upon cooling from the melt, except under very special conditions. However, one of the most fascinating possibilities in the study of the magnetic molten salts is that the liquids can be mixed somewhat arbitrarily. To give some idea of the application of this to our linewidth studies we report on some arbitrary mixtures of KMnF_3 and MnF_2 in the molten state. Now, in general, these do not exist as compounds with a specific crystal structure in the solid state. The phase diagram for the system $\text{KF}:\text{MnF}_2$ has not been reported but it is common practice to extrapolate information relative to it from the known²⁸ $\text{KF}:\text{MgF}_2$ diagram, with appropriate changes made for the differences in melting temperatures for the pure compounds. On the Mn-rich side there apparently exists no other homogeneous compound in between MnF_2 ($T_m = 930^\circ\text{C}$) and the congruently melting double fluorides $\text{KF}:\text{MnF}_2$ ($T_m = 1013^\circ\text{C}$). Of course, there may be at least one eutectic in this region. Thus in general we may expect an arbitrary mixture of KMnF_3 and MnF_2 to be a "uniform" liquid at high temperatures, but below T_{m1} ($\leq 1013^\circ\text{C}$) precipitation of KMnF_3 would occur. Finally below some temperature T_{m2} the mixture would condense into crystalline regions of KMnF_3 and MnF_2 , in proportion to the original relative compositions.

A specific example of the molten-state linewidth measurement for a mixed system is shown in Fig. 8 for the mixture 1.56MnF₂:1KMnF₃. All of the data shown were taken in cooling from the highest temperature (1200°C). In the completely molten phase ($T_{m1} \approx 970^\circ\text{C}$) the linewidth is seen to be intermediate in magnitude between that of MnF₂ and KMnF₃ at all temperatures and, with regard to the slope of ΔH with increasing T , also shows a monotonic decrease as one moves upward in T away from T_{m1} .

As to the results obtained in the solid phase for "flash-frozen" arbitrary mixtures, one could discern at 300 K the superposition of MnF₂ and KMnF₃ line profiles (because of their very different width) in proportion to the relative concentrations. The data shown in Fig. 8 ($T < 970^\circ\text{C}$) for the mixture 1.56MnF₂:1KMnF₃ indicate a discontinuity in ΔH at T_{m1} and a further decrease as T decreases, with the error bars showing the uncertainties that arise because of the non-Lorentzian behavior in the mixed molten-solid phase, particularly in the region $T_{m2} < T < T_{m1}$.

3. Dependence of $\Delta H(T_m)$ on concentration of magnetic ions

The similarities in the linewidths of all three double fluorides (KMnF₃, RbMnF₃, CsMnF₃) at T_m , as contrasted with their differences in the solid state, suggest that $\Delta H(T_m)$ might well be correlated with the average magnetic ion density in the liquid. We assume that at, or just slightly above, T_m the viscosity is quite similar for all of the molten salts under consideration. Hence, it is reasonable to compare ΔH at T_m for different salts with various concentration of magnetic ions.

With this in mind, we have examined the linewidth at T_m , $\Delta H(T_m)$, for several magnetically diluted salts to effect a comparison with the magnetically dense ones. We show the results in Fig. 9, in a log-log plot of $\Delta H(T_m)$ versus concentration of magnetic ions (i.e., Mn²⁺). For these purposes the concentration c is defined as the Mn²⁺ ion fraction of the total cation density (e.g., MnF₂ [100%] and KMn_{0.01}Mg_{0.99}F₃ [0.5%]). One striking difference between the concentration-dependent results in the solid and molten states is immediately apparent from a comparison of Figs. 6 and 9. In the solid, magnetic dilution results in a slow initial decrease of ΔH with c . But at a relatively high value of c [(20–30)%], the linewidth then begins to increase rapidly as c decreases until, finally, a resolved hfs appears (see Fig. 5). In the molten state the rapid decrease in ΔH with magnetic dilution is not arrested until a much smaller concentration [(1–2)%], following which a rapid broadening occurs with further decrease of c .

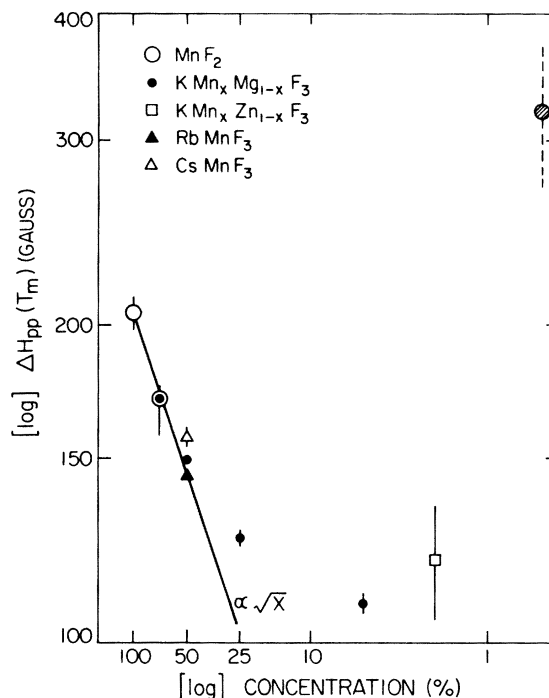


FIG. 9. Dependence of the linewidth on the Mn percentage per all cations for several fluoride melts near the melting point. The most dilute sample (0.5 cation %, represented by the hatched symbol) approaches the sensitivity limit for the measuring procedure generally used in the present investigation.

Concerning the dilute extreme of the concentration-dependent studies, a number of attempts were made to observe hfs (⁵⁵Mn and/or ¹⁹F) on the EPR signal in the molten state—but all without success. The sample shown as 0.5% on the extreme right of Fig. 9, KMn_{0.01}Mg_{0.99}F₃, showed none. No signal whatsoever could be observed in our apparatus for a sample of nominal concentration $c = 0.05\%$ (KMn_{0.001}Mg_{0.999}F₃), even with the use of long-time signal-averaging techniques. However, one could reversibly reproduce the spectrum of Fig. 5(e) in this sample when $T < T_m$. Using an improved microwave spectrometer²⁹ and slightly different experimental techniques³⁰ we were able to observe EPR in the molten state of a sample of KMn_{0.0003}Mg_{0.9997}F₃. However, in the temperature region $T_m \leq T < T_m + 150^\circ\text{C}$ only a weak, structureless, non-Lorentzian-shaped line could be discerned with a peak-to-peak derivative width of $\Delta H_{pp} \approx 460 \pm 30\text{G}$. The absence of hfs in a sample with Mn²⁺ concentration as small as $c = 0.015\%$ in the molten fluorides appears to be irrefutable.

IV. THEORY AND INTERPRETATION

In the following discussion of the interpretation of the observed EPR linewidths we are led to quite

different considerations for (i) the dense paramagnets in the solid state, (ii) the magnetically diluted systems in the solid state, and (iii) the molten materials.

A. Linewidths of the dense paramagnets: $T < T_m$

In the dense solid paramagnet at or below the Debye temperature Θ_D it is ordinarily sufficient to treat the EPR linewidth as arising from dipolar and exchange interactions between spins *rigidly* localized at their lattice positions. However, because these interactions are sensitively dependent on ionic separations it may be necessary, at least well above Θ_D , to include the effects of ionic motion—in the form of phonons and thermal expansion. In addition, there is the possibility that ion diffusion, ion interchange, or even the “melting” of one ionic sublattice (as occurs in superionic conductors) might lead to changes in the linewidth that are not expected within the framework of rigid-lattice spin-dynamical theories.

In certain cases (e.g., MnO and MnS) the observed high-temperature behavior of the EPR linewidth does find ready explanation³¹ in terms of a rigid-lattice theory. These face-centered-cubic paramagnets have strongly competing exchange interactions producing unusually large short-range-order effects that cause the linewidths to be very temperature dependent even well above the ordering temperature. In the paramagnets we have studied (e.g., KMnF_3 and MnF_2), only one exchange interaction predominates. Nevertheless the large spin-dynamical effects on the temperature dependence of linewidths in MnO and MnS suggest that we first examine the rigid-lattice predictions in our systems, as well. Hence, in the Appendix we explore two such theories, involving quite different approximations in treating the spin dynamics: (i) a perturbative approach of the sort introduced by Mori and Kawasaki⁵ and by Mori⁶; here we treat the static spin correlations in a mean-field approximation modified to include the effects of short-range order in self-consistent fashion using the Onsager “reaction-field” concept, and (ii) the dynamical Green’s-function theory of Tomita and Tanaka.^{8,9} Explicit calculations are made there for the simple cubic magnetic lattice (appropriate to KMnF_3 or RbMnF_3). We find that only a very small part of the *observed* high-temperature variation of ΔH can be explained in this way (see Fig. 10). Moreover, *any* rigid-lattice theory must have a regular high-temperature expansion, with a leading term proportional to J/T , which will be overwhelmingly dominant at temperatures well above zJS/k_B . Thus for a linewidth which grows with increasing temperature this pre-

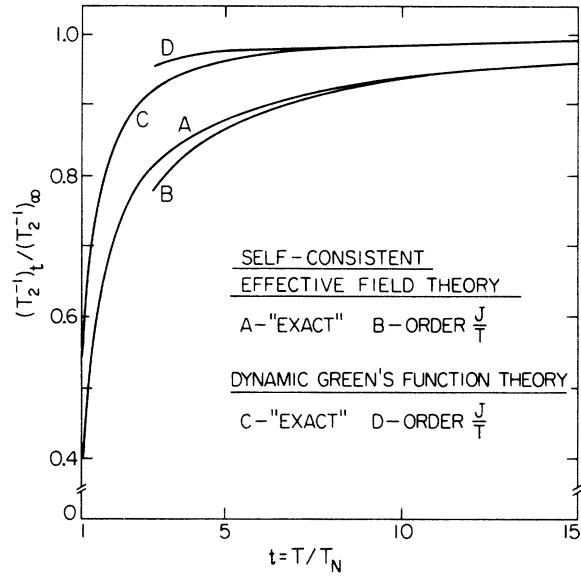


FIG. 10. Comparison of the spin-dynamical predictions of two rigid-lattice theories for the temperature dependence of the EPR linewidth (normalized to its infinite-temperature value) for a simple cubic paramagnet with only nearest-neighbor antiferromagnetic exchange interactions. Curve A represents the self-consistent effective-field-theory results [Eq. (A17) divided by Eq. (A18)] and B is the leading term in the high-temperature expansion of the same theory [see Eq. (A19)]. Curve C is the dynamical Green’s-function theory [Eq. (A22)] and D the corresponding leading term in the high-temperature expansion [see Eq. (A23)].

dicts a negative curvature for the ΔH -vs- T curve, in *qualitative* disagreement with the observed (see Fig. 3) positive or zero curvature at higher temperatures. The abrupt decrease of ΔH in MnF_2 several hundred degrees below T_m (see Fig. 4) is even more clearly outside the range of behavior possible in a rigid-lattice theory. Therefore we must relax the constraint of lattice rigidity if we are to understand the high-temperature behavior of EPR linewidths in the materials studied here.

1. Effects of lattice vibrations

Independent of the particular approximations of a given theory of the rigid-lattice spin-dynamical effects on the EPR linewidth of an exchange-coupled paramagnet, very general perturbation arguments suggest that $\Delta H \propto D^2/\omega_e$, where D and ω_e are measures of the dipole and exchange interaction strengths, respectively. Different approximate theories lead to specific weightings of the spatial Fourier components of these interactions (see Appendix). The lattice vibrational modulation of these components is conveniently separated into

the static thermal-expansion effect (anharmonicity) and the dynamic harmonic effects.

The harmonic motion about the thermal equilibrium positions effectively introduces time dependence into the Hamiltonian. Because the characteristic lattice vibration time set by the Debye energy ($\tau = \hbar/k\Theta_D \sim 10^{-13}$ sec) is very short compared to the EPR relaxation time T_2 , we can average over the ionic motion. Furthermore, we claim that in these strongly exchange-narrowed materials we can separately average the dipolar and exchange factors in $\Delta H \propto D^2/\omega_o$: Consider a spin S_o at a particular lattice site o . Its contribution to $1/T_2$ is governed by the power spectrum of its dipolar interactions with other spins S_n —i.e., of $D(t)D(0)$, where the temporal fluctuations of $D(t)$ arise from phonon modulation of the vector \vec{R}_{on} connecting sites o and n . This power is reduced by the fluctuation of the spin S_n , which primarily results from the exchange interactions J_{nl} it has with its z nearest neighbors, at sites l . The phonon modulation of J_{nl} at T is largely independent of the modulation of the geometrical factors in the dipole interaction between S_o and S_n , since the site o is, *at most*, only one of the z nearest neighbors exchange coupled to S_n . Thus the phonon-induced dipolar fluctuations are to a very good approximation uncorrelated with the corresponding harmonic variations of the exchange interactions.

Since the characteristic vibrational frequencies of the lattice, particularly at high temperatures, are of order $\omega_D = k\Theta_D/\hbar$ and ω_D is larger than either ω_o or D , it is proper to time average the latter two quantities over the lattice vibrations. Because of the arguments given above concerning the lack of correlation we separately average D^2 and ω_o ; hence, $1/T_2 \propto \langle D^2 \rangle / \langle \omega_o \rangle$. These rough arguments find more precise justification in a moment analysis of ΔH which explicitly includes the lattice vibrational time dependence of the exchange and dipolar contributions to the Hamiltonian. Likewise, an examination of the self-consistent effective-field theory (see Appendix) in which the sources of the time dependence can be followed at each stage, leads to the same conclusion.

A rigorous treatment of the problem would require, first, having detailed information on the phonon modes for these rather complex lattices and, second, knowledge of the angular and distance dependence of the superexchange interaction. (The dependence of the classical dipole-dipole interaction, of course, is known.) For purposes of estimating the magnitudes of the corrections that need be applied over the temperature region of interest we content ourselves with a

relatively simple model instead. We follow the general approach used by Bloch and Georges³² in studying the temperature dependence of the superexchange interaction. We treat the temperature dependence of both the dipolar and exchange interactions as due only to changes in the magnitude of the relative separations of the magnetic ions and not to the angular displacements nor to the relative positions of magnetic and ligand ions. We then Taylor-series expand

$$\begin{aligned} \langle f(R) \rangle &\approx f(R_0) + f'(R_0) \langle z - R_0 \rangle \\ &\quad + [f''(R_0)/2R_0] (\langle x^2 \rangle + \langle y^2 \rangle) \\ &\quad + \frac{1}{2} f'''(R_0) \langle (z - R_0)^2 \rangle, \end{aligned} \quad (4.1)$$

where \vec{R}_0 is the zero-temperature equilibrium vector connecting a pair of magnetic ions, z is parallel to \vec{R}_0 , and $\langle x^2 \rangle + \langle y^2 \rangle$ is the mean-square deviation perpendicular to \vec{R}_0 . In the harmonic approximation $\langle z - R_0 \rangle = 0$ at all temperatures, and

$$\begin{aligned} \langle x^2 \rangle &= \frac{\hbar}{mN} \sum (\hat{x} \cdot \vec{\epsilon}_{k\alpha})^2 (2n_{k\alpha} + 1) \\ &\quad \times (1 - e^{i\vec{k} \cdot \vec{R}_0}) \omega_{k\alpha}^{-1}, \end{aligned} \quad (4.2)$$

where the sum is over wave vectors \vec{k} in the first Brillouin zone and over all phonon branches α . Here m is the mass of a magnetic ion, $\omega_{k\alpha}$ is the frequency of the phonon with wave vector \vec{k} and polarization α , and $n_{k\alpha} = (e^{\beta\hbar\omega_{k\alpha}} - 1)^{-1}$ is the equilibrium occupation number of that mode. $\vec{\epsilon}_{k\alpha}$ is the polarization vector appropriate to the motion of the magnetic ion; it is normalized by $\sum |\vec{\epsilon}_{k\alpha}(s)|^2 = 1$, where s labels the atoms in a unit cell.

Lacking detailed knowledge of $\vec{\epsilon}_{k\alpha}$ as well of $\omega_{k\alpha}$, we turn to a simple model. The factor $(2n_{k\alpha} + 1)/\omega_{k\alpha}$ favors low-energy acoustic modes over higher-energy optical modes for the same value of k . We then consider only acoustic branches and take $|\vec{\epsilon}_{k\alpha}|^2 = m/M$, where M is the mass of the unit cell, as is the case for small- k acoustic phonons, where atoms within a unit cell move in phase with equal amplitudes. We further take a Debye spectrum $\omega_k = v_s k$, with v_s independent of both propagation direction and polarization of the phonon. Within this approximation

$$\begin{aligned} \langle x^2 \rangle &= \langle y^2 \rangle = \langle (z - R_0)^2 \rangle \\ &= \frac{\hbar}{2\pi^2 \rho v_s} \int_0^{k_D} (2n_k + 1) \left(1 - \frac{\sin kR_0}{kR_0} \right) k dk, \end{aligned} \quad (4.3)$$

where ρ is the mass density. At high temperatures ($T \gg \Theta_D$) we have $\beta\hbar\omega_k \ll 1$ and $n_k \approx (\beta\hbar\omega_k)^{-1}$, so

$$\langle x^2 \rangle \approx \frac{k_D}{\pi^2 \rho \beta v_s^2} \left(1 - \frac{s(k_D R_0)}{k_D R_0} \right), \quad (4.4)$$

where $s(x)$ is the sine integral:

$$s(x) = \int_0^x dy \frac{\sin y}{y}.$$

If we allow for anharmonic forces we have, by definition

$$\begin{aligned} \langle z - R_0 \rangle &= R_0 \left(\exp \int_0^T \alpha_L(T) dT - 1 \right) \\ &\approx R_0 \int_0^T \alpha_L(T) dT, \end{aligned} \quad (4.5)$$

where $\alpha_L(T) \equiv (1/L)(\partial L/\partial T)$ is the (temperature-dependent) coefficient of linear expansion; we assume its value is obtainable directly from other measurements. The anharmonic corrections to the mean-square deviation, both from thermal expansion and from an effective softening of the force constants, are collectively small higher-order effects, which we shall neglect.

There now exists strong empirical evidence^{33, 34} that in many of the transition-metal fluorides and oxides the distance dependence of the superexchange interaction follows an approximate relation

$$\left(\frac{\partial \ln J}{\partial \ln R} \right)_{R_0} \approx -10 \quad (4.6)$$

for small changes in R about R_0 . Furthermore, $\bar{D}(q)$ the geometric dipolar factor [see, e.g., Eq. (A9)] is the Fourier transform of terms which fall off with distance as R^{-6} . Then from the expansions discussed above we have

$$\frac{\langle D(q) \rangle_T}{\langle D(q) \rangle_{300}} \approx 1 - 6 \int_{300}^T \alpha(T') dT' + 15C(T - 300) \quad (T \gg \Theta_D), \quad (4.7a)$$

where

$$C = \frac{k_D k_B}{\pi^2 \rho v_s^2 a_0^2} \left(1 - \frac{s(k_D a_0)}{k_D a_0} \right)$$

and a_0 is the near-neighbor separation. Similarly,

$$\frac{\langle \omega_e \rangle_T}{\langle \omega_e \rangle_{300}} \approx 1 - 10 \int_{300}^T \alpha(T') dT' + 45C(T - 300). \quad (4.7b)$$

For RbMnF_3 we may use the known elastic constants³⁵ to estimate the relevant parameters in the harmonic contributions in Eqs. (4.3) and (4.4): $v_s \approx 5 \times 10^5$ cm/sec. [direct measured values are R and α dependent; this value is based on Θ_D (elastic)]: $a_0 = 4.2 \times 10^{-8}$ cm; $k_D a_0 = 3.9$; $\rho = 4.4$ g/cm³; $1 - s(k_D a_0)/k_D a_0 = 0.54$; which gives $C \approx 3.6 \times 10^{-7}$. The variation of the lattice parameter in KMnF_3 between room temperature and the melting point has recently been measured directly by neutron elastic scattering.³⁶ The results are well fit over the whole of the measured tempera-

ture range by choosing

$$\alpha_L(T) = 14.3 \times 10^{-6} + 7.4 \times 10^{-9} T \quad (\text{KMnF}_3, T \geq 300 \text{ K}). \quad (4.8)$$

We assume this to be a reasonably accurate representation for RbMnF_3 in this same temperature region, as well. Then using Eqs. (4.7) we find

$$\begin{aligned} \langle \langle \bar{D}(q) \rangle_T - \langle \bar{D}(q) \rangle_{300} \rangle / \langle \bar{D}(q) \rangle_{300} \\ \approx - [9.9 \times 10^{-5} (T - 300) + 2.2 \times 10^{-8} (T - 300)^2] \\ + 5.4 \times 10^{-6} (T - 300), \end{aligned} \quad (4.9a)$$

$$\begin{aligned} \langle \langle \omega_e \rangle_T - \langle \omega_e \rangle_{300} \rangle / \langle \omega_e \rangle_{300} \\ \approx - [16.5 \times 10^{-5} (T - 300) + 3.7 \times 10^{-8} (T - 300)^2] \\ + 1.6 \times 10^{-5} (T - 300), \end{aligned} \quad (4.9b)$$

where, in each case, the first (negative) term is the contribution from thermal expansion and the second (positive) term arises from harmonic vibrations. The latter contributions, whose values are relatively more uncertain because of the several approximations required, are substantially smaller than the anharmonic terms. This is in contrast to the near cancellation of the two effects obtained by Bloch and Georges in the superexchange calculation in the transition-metal oxides.³² Over the temperature range from 300 K to the melting point in RbMnF_3 we find for the lattice-vibration-induced changes

$$\begin{aligned} \delta \langle \bar{D}(q) \rangle / \langle \bar{D}(q) \rangle &\approx -11.6\%, \\ \delta \langle \omega_e \rangle / \langle \omega_e \rangle &= \delta J / J \approx -18.6\%, \\ \delta \langle \Delta H \rangle / \Delta H &\approx 7\%. \end{aligned}$$

The major uncertainty in these estimates is in the approximate relation (4.6) expressing the distance dependence of J . A recent calculation³⁷ of the dependence of J on interion separation for the linear configuration $\text{V}^{2+} - \text{F}^- - \text{V}^{2+}$, using the methods developed by Huang and Orbach,³⁸ show $(\partial \ln J / \partial \ln R)_{R_0} \approx -12$. It is important to realize that $\partial \ln J / \partial \ln R$ may vary appreciably as the lattice expands and that ultimately a more direct measurement of J as a function of T will be required for the complete interpretation of the linewidth experiments. Notwithstanding all of the above we feel it worthwhile to qualitatively estimate the anharmonic and harmonic vibrational corrections so as to ascertain whether the effects they produce are indicative of the major discrepancies between theory and experiment. In anticipation of doing that, it might be remarked that in the RbMnF_3 , KMnF_3 , and CsMnF_3 lattice vibrational effects alone are probably responsible for the difference between theory and ex-

periment in the high-temperature regime but in MnF_2 they clearly are not.

2. Ion diffusion effects

The thermally activated diffusive motion of atoms may result in nuclear spin-lattice relaxation and the narrowing of dipolar-broadened resonances, both in the solid and liquid states. Beginning with the pioneering work of Bloembergen, Purcell, and Pound³⁹ on liquids, until the NMR studies of Eisenstadt and Redfield⁴⁰ on vacancy diffusion of Li and F in solid LiF, an extensive literature has developed⁴¹ on motion-related resonance phenomena. To our knowledge no detailed theoretical or experimental study of the combined effects of exchange and motional narrowing has been made, although some fundamental differences in the two phenomena have been recognized.⁴² We believe the narrowing of the EPR in MnF_2 well below the melting point and, in particular, the fact that the anisotropy in the linewidth $(1 - \Delta H^{\parallel} / \Delta H^{\perp})$ changes sign in this temperature region, is indicative of a one-dimensional interchange motion of the Mn^{2+} ions along the c axis. We turn now to a qualitative discussion of simultaneous motional and exchange narrowing effects.

In the absence of exchange forces, the random walk of an atom will cause a narrowing of the dipole broadening of the resonance to occur when the correlation time τ_c of the relative motion becomes appreciably less than $\langle(\omega - \omega_0)^2\rangle^{-1/2}$, where $\langle(\omega - \omega_0)^2\rangle$ is the second moment of the rigid-lattice line profile $I(\omega - \omega_0)$. The behavior of the linewidth $1/T_2$ in the extreme narrowing limit can be deduced from the approximate expression

$$1/T_2 \approx \langle(\omega - \omega_0)^2\rangle \tau_c / (1 + \omega_0^2 \tau_c^2).$$

When $\tau_c \ll \omega_0^{-1}$, as well as satisfying the inequality mentioned above, then the linewidth depends only on the thermodynamic properties of the system that cause the correlation time of the motion to vary and *not* on the frequency for resonance:

$$1/T_2 = \langle(\omega - \omega_0)^2\rangle \tau_c. \quad (4.10a)$$

Now in the presence of strong exchange forces and no motion we have seen that $1/T_2 \approx \langle(\omega - \omega_0)^2\rangle \tau_{\text{ex}}$. If we initially postulate that the diffusive motion of the ions is not correlated with the exchange forces then we can immediately see there are two extreme regions in which the narrowing processes would be well delineated (we introduce the symbol τ_m for the correlation time for motion):

(i) $\tau_m \gg \tau_{\text{ex}}$: The spin-correlation functions would decay via the exchange interactions before appreciable diffusive motion would take place; then

$$1/T_2 \approx \langle(\omega - \omega_0)^2\rangle \tau_{\text{ex}}. \quad (4.10b)$$

(ii) $\tau_m \ll \tau_{\text{ex}}$: Before exchange forces could become operative the motion would cause a given spin to become uncorrelated with another in a time $\approx \tau_m$; then

$$1/T_2 \approx \langle(\omega - \omega_0)^2\rangle \tau_m. \quad (4.10c)$$

In the simplicity of these two extreme statements there is contained an important fact, namely, that motion will have no significant effect on the narrowing process until $\tau_m < \tau_{\text{ex}}$. But $\tau_{\text{ex}} \approx 0.6 \times 10^{-12}$ sec for MnF_2 . One can show, from simple order-of-magnitude estimates and the experimental results on the NMR in LiF, that the characteristic jump frequencies ω_j associated with the diffusive motion of *vacancies* will be at least 10^4 times too slow to allow for $\tau_m^{-1} \geq \tau_{\text{ex}}^{-1}$. For example, thermally activated vacancy diffusion, in the intrinsic region, may be characterized by the relation

$$\omega_j = \omega_a e^{-\Delta/kT}, \quad (4.11)$$

where ω_a , the attempt frequency, will not exceed 10^{14} sec⁻¹ and Δ is a quantity which includes the energy necessary to create a vacancy and the barrier for the hopping of an ion into a vacant site minus T times the entropy of disorder associated with vacancies being present.⁴³ For divalent cation vacancy diffusion it would be generous to take Δ to be as small as 1 eV, from which one immediately deduces $\omega_j \approx 1/\tau_c \approx 3 \times 10^9$, for $T = 1100$ K. In LiF both ω_j^{Li} and ω_j^{F} are much less than 10^8 sec⁻¹ at $T = 1100$ K.

Moreover, recent measurements⁴ of the electrical conductivity of MnF_2 up to the melting point T_m show that whatever the mechanism is for ionic conductivity (vacancy or interstitially hopping) no characteristic jump frequency above 10^8 Hz is present below T_m . Thus *no* mechanism which involves charge transport and therefore contributes to the electrical conductivity can be involved in the motional narrowing of the MnF_2 EPR below T_m .

That the energy to create a vacancy is large is seen to be the main impediment to diffusive motional narrowing. On the other hand, one mechanism for motion does exist which might have a lower effective barrier and at the same time not contribute to the electrical conductivity—direct *interchange*⁴⁴ of two cations. The open structure of the rutile lattice and the close proximity of nearest-neighbor Mn ions suggest that this could well be a mechanism for motional narrowing of the EPR as $T \rightarrow T_m$.

One can quantify these remarks with regard to MnF_2 as follows: Suppose we consider a lattice of magnetic dipoles all with spin $S = \frac{1}{2}$. Then the physical interchange of any two spins is indis-

tinguishable from a bilinear scalar exchange interaction $\vec{S}_i \cdot \vec{S}_j$ between the same pair, assuming the corresponding correlation times to be identical. [In general, the spin operator equivalent for the interchange of two spins with $S > \frac{1}{2}$ will require the inclusion of terms up to and including $(\vec{S}_i \cdot \vec{S}_j)^{2S}$.] Hence one might expect that an understanding of the narrowing and the reversal in sign of the anisotropy in the linewidth as $T \rightarrow T_m$ could be modeled in terms of an increase in the "effective" exchange interaction but resulting, in fact, from the physical interchange of near-neighbor (nn) Mn^{2+} ions in a thermally activated process.

The magnitude and particularly the anisotropy of the EPR linewidth in MnF_2 , well below T_m , may be deduced from the calculations of the second (M_2) and fourth (M_4) moments of the line profile. Using the values for M_2 and M_4 with $\vec{H}_0 \parallel \vec{c}$ and $\vec{H}_0 \perp \vec{c}$ and the fact that, in the extreme narrowing limit, $\Delta H \propto M_2(M_2/M_4)^{1/2}$, one finds $\Delta H^{\parallel} = 1.1 \Delta H^{\perp}$. Because the rigid-lattice width $\Delta H \propto M_2^{1/2}$ in the absence of exchange would also have the same sense to the anisotropy this might not seem surprising at first. However, a detailed analysis²³ shows that the anisotropy in M_4 results from the fact that $z_{\text{nnn}} J_{\text{nnn}} \gg z_{\text{nn}} J_{\text{nn}}$.⁴⁵ If the effective near-neighbor exchange J_{nn} is increased so that the above inequality is reversed, the sense of the anisotropy in M_4 and in the linewidth is also reversed; i.e., $\Delta H^{\parallel} < \Delta H^{\perp}$! We have considered the possibility that the true J_{nn} could increase with temperature and produce the observed effects on ΔH and obviate the need for the interchange mechanism. But the magnitude of the required change and the rapidity with which it would have to take place as a function of temperature are both so large that we are led to believe this to be a highly unlikely explanation of the experimental observations. Furthermore, neutron-diffraction measurements show no anomalies in the lattice constants in this temperature region.³⁶

A crude estimate of the interchange activation energy required to affect this may be deduced as follows: At the temperature where the anisotropy in the linewidth disappears ($T_0 \approx 1100^\circ\text{K}$) one might expect that $\tau_j = \tau_{\text{ex}}$. Hence $\nu_j = (\tau_{\text{ex}})^{-1} = \nu_a e^{-\Delta/kT_0}$ and taking $\nu_a \approx 4.8 \times 10^{13}$ Hz, $(\tau_{\text{ex}})^{-1} = 1.6 \times 10^{12}$ Hz, we find a value of $\Delta = 0.32$ eV. We believe this to be a not unreasonable value for the near-neighbor Mn^{2+} interchange activation energy in the vicinity of the melting point. Since one does not first have to create a vacant site into which the diffusing ion can jump in an activated manner, one might expect that $\Delta_{\text{interchange}} < \Delta_{\text{vacancy}}$. A somewhat more quantitative analysis is given in the following section.

One further point can be inferred from the de-

tailed theory given by Eisenstadt and Redfield⁴⁰ for the anisotropy in the linewidth of a random-walk diffusion on a cubic lattice. If the motion is random in three dimensions then the anisotropy in the rigid-lattice linewidth is preserved both in sign and, qualitatively, in magnitude. Thus apart from the formal identification of the specific motion along the c axis with an effective near-neighbor exchange in MnF_2 we believe that a random walk on the three-dimensional body-centered-tetragonal cation lattice would produce further narrowing but not reverse the sign of the anisotropy of the linewidth.

The absence of similar motional narrowing in the XMnF_3 compounds is presumably associated with a higher activation energy for the interchange of cations. From a topological point of view this is not surprising since nn Mn^{2+} ions have a large F-ion midway on the line joining them and nnn Mn^{2+} ions are much too far apart.

3. Interpretation of the experimental results on the dense paramagnets

The conclusions to be drawn from the previous sections are that, in KMnF_3 and RbMnF_3 (and probably in CsMnF_3), lattice vibrations and expansion dominate the temperature dependence of the linewidth, and in MnF_2 a thermally activated ion diffusion causes the linewidth behavior at high temperatures. We now give some quantitative implications of the above.

(a) *Temperature dependence of the exchange interaction in KMnF_3 and RbMnF_3* : Having concluded (see Appendix) that the Tomita-Tanaka theory⁸⁻¹⁰ is preferable for quantitative comparisons with the experiment we now proceed as follows: Rather than make anharmonic and harmonic lattice corrections to both the dipolar and exchange interactions to normalize the experimental results to this "rigid-lattice" theory, we choose to apply only the dipolar corrections and then deduce the variation of the exchange interaction with temperature from the comparison of experiment with theory. The motivations for this are obvious. The spin dynamical effects in the theory could lead to changes in ΔH of no more than 3% between $T = 5T_n$ and the melting point, whereas the experimentally observed changes (~15%) in this region are much larger. Clearly, the experiments can *not* be used as a test of the spin dynamics.

In addition, within the framework of the model discussed in Sec. IV A 1, there is less uncertainty in applying the dipolar corrections resulting from lattice dynamical effects as compared with the corresponding exchange ones. Hence we elect to

TABLE II. Linewidth data versus temperature for KMnF_3 and RbMnF_3 for approximately $5 \leq T/T_n \leq 15$. We give in columns 2, the smoothed raw data; 3, the data corrected for the variation of the dipolar interactions as a result of lattice expansion and vibrations; 4, the "rigid-lattice" spin-dynamical theory of Refs. 8 and 9 normalized to the 400-K value of column 3; and 5, the change in the exchange interaction with temperature deduced from dividing entries under 4 by the corresponding ones under 3.

1 T ($^{\circ}\text{K}$)	2 $\Delta H(\text{G})_{\text{exp}}$		3 $\Delta H(\text{G})_{\text{d.c.}}$		4 TT theory		5 $\frac{J(T)}{J(400\text{ K})}$	
	K	Rb	K	Rb	K	Rb	K	Rb
400	63.1	62.8	65.3	65.0	65.3	65.0	1.000	1.000
500	64.3	63.6	67.2	66.5	66.2	65.6	0.984	0.987
600	65.4	65.1	69.0	68.7	66.6	66.0	0.965	0.960
700	66.8	66.8	71.2	71.2	67.0	66.5	0.940	0.933
800	68.2	68.4	73.5	73.7	67.2	66.5+	0.922	0.903
900	69.9	69.0	76.1	75.2	67.4-	66.7	0.885	0.887
1000	71.8	71.5	79.1	78.7	67.4+	66.8	0.853	0.849
1100	73.8	73.0	82.2	81.3	67.5	66.9	0.822	0.823
1200	76.1	75.8	85.7	85.4	67.6	67.0	0.789	0.785

use theory and experiment to deduce the temperature dependence of J with the hope that it will elucidate further the dependence of J on interion separation and angle.

For the above purpose we have smoothed the experimental data for KMnF_3 and RbMnF_3 to give a best fit. The refined data so obtained, at 100° intervals beginning at 400 K are shown in Table II. These are subsequently corrected for changes in the dipolar interaction. A comparison between the Tomita-Tanaka (TT) rigid-lattice theory [Eq. (A22)], normalized to the 400 K dipolar-corrected value, may be had from an examination of columns 3 and 4 in Table II. Dividing corresponding entries in those two columns we obtain $J(T)/J(400\text{ K})$ vs T which is given in column 5 and plotted for both compounds in Fig. 11. For purposes of illustration the "expected" variation in $J(T)/J(400\text{ K})$, assuming a $J \propto (R - R_0)^{-n}$ dependence, with $n=12$, is shown in the same figure as a small dashed line.

We also display in Fig. 11 by the dashed line what the variation in $J(T)/J(400\text{ K})$ would be if we assumed there were no temperature-dependent spin dynamical contributions to ΔH above 400 K. The reason for doing this is that both of the spin dynamical theories considered clearly overestimate the dependence of ΔH in the lower-temperature region. In fact, between $2 \leq T/T_n < 5$ both KMnF_3 and RbMnF_3 have almost no temperature dependence to ΔH ! One might argue that in this latter region, where lattice vibrational contributions are very small ($T < \Theta_D$), if ΔH does not vary appreciably with T it will vary even less at higher T from purely spin dynamical effects! Nevertheless, it is clear from the curves of Fig. 11 that the qualitative variation in $J(T)/J(400^{\circ}\text{K})$ is not changed

significantly by these considerations.

(b) *Analysis of the high-temperature behavior of the MnF_2 linewidth.* Having reasoned before that the rapid decrease in ΔH with increasing T above 600°C —as well as the reversal of its anisotropy—probably has its origin in a thermally activated Mn ion interchange, we proceed to extract

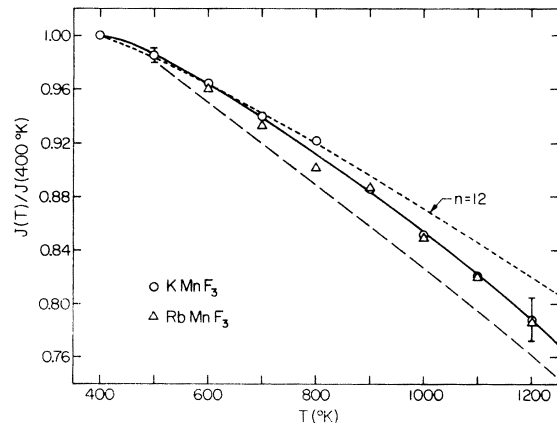


FIG. 11. Temperature dependence of the exchange interaction (normalized to its 400-K value) for KMnF_3 and RbMnF_3 . The values shown are deduced from the EPR linewidth measurements after first correcting only the dipolar interaction for phonon-induced effects (both harmonic and anharmonic) and then comparing the predictions of the dynamical Green's function with the "corrected" experimental observations. (See Table II and Secs. IV A and IV B.) The large dashed curve represents the same calculation but with no temperature dependence assumed to the rigid lattice linewidth. The solid curve is a best fit to the combined KMnF_3 - RbMnF_3 data. The small dashed curve is a plot of $J(T)/J(400\text{ K})$ assuming J varied as $(R - R_0)^{-n}$ with $n=12$.

the barrier energy from a simple model.

In the absence of a detailed theory for the combined effects of exchange and ion interchange on the EPR linewidth, we model the spin dynamical behavior by analogy with what happens when there are two exchange interactions, say J_1 and J_2 . It is known in the latter instance the decay of $\langle S_i(t)S_j(0) \rangle$ is governed by an effective exchange frequency⁴⁶

$$\omega_e^2 = \frac{2}{3} \hbar^{-2} S(S+1) (z_1 J_1^2 + z_2 J_2^2) \equiv \omega_{e_1}^2 + \omega_{e_2}^2. \quad (4.12)$$

Since $\Delta H \propto D^2 \omega_e^{-1}$, we would expect that if one exchange interaction (say, J_2) were replaced by an ion interchange process characterized by a hopping frequency ω_h , the new effective frequency would be given by

$$\omega_{\text{eff}}^2 = \omega_{e_1}^2 + \omega_h^2 \quad (4.13)$$

and $\Delta H \propto D^2 \omega_{\text{eff}}^{-1}$. It follows that the linewidth may be expressed as

$$[(\Delta H)_0 / \Delta H]^2 - 1 = (\omega_h / \omega_{e_1})^2, \quad (4.14)$$

with $(\Delta H)_0$ being the linewidth in the absence of hopping. Assuming the hopping to be described by an Arrhenius relation [as in Eq. (4.11)]

$$\omega_h = \omega_a e^{-E_0/kT}, \quad (4.15)$$

where ω_a is the attempt frequency and E_0 is the interchange barrier energy we find

$$[(\Delta H)_0 / \Delta H]^2 - 1 = (\omega_a / \omega_{e_1})^2 e^{-2E_0/kT}. \quad (4.16)$$

In this form the prefactors to the exponential and E_0 are usually assumed to have negligible temperature dependence.

Figure 12 shows a semilog plot of $[(\Delta H)_0 / \Delta H]^2 - 1$ vs $1/T$ for the case of $\vec{H}_0 \parallel \vec{c}$. To obtain the plot we first extrapolated the linewidth below 400 °C to higher temperatures using the Tomita-Tanaka approach for the body-centered-tetragonal spin lattice, retaining only the leading J/kT term $[(1/T_2)_T / (1/T_2)_\infty = 1 + 0.17T_c^2/T]$; compare this with Eq. (A23) for the sc lattice]. This we label as $(\Delta H)_0$ in the inset to the main figure. (We assume lattice expansion effects on ΔH for MnF_2 to be much smaller than in KMnF_3 and RbMnF_3 .⁴⁷) Next, we smooth the data by drawing a "best fit" curve through the experimental points. Then for the semilog plot "data" were selected from the smoothed curve at 25° intervals beginning at $T = 600^\circ \text{C}$ (873K).

From the initial (lower temperature) behavior an activation energy $E_0 = 0.34 \text{ eV}$ is obtained and, assuming $\omega_{e_1} \approx 10^{12}/\text{sec}$, we derive a value of $\omega_a = 1.3 \times 10^{13}/\text{sec}$. The latter is not unreasonable. As T approaches the melting point, the more rapid decrease in ΔH than is predicted by Eq. (4.14) probably is indicative of several not unrelated effects: (i) when ω_h becomes comparable with ω_e

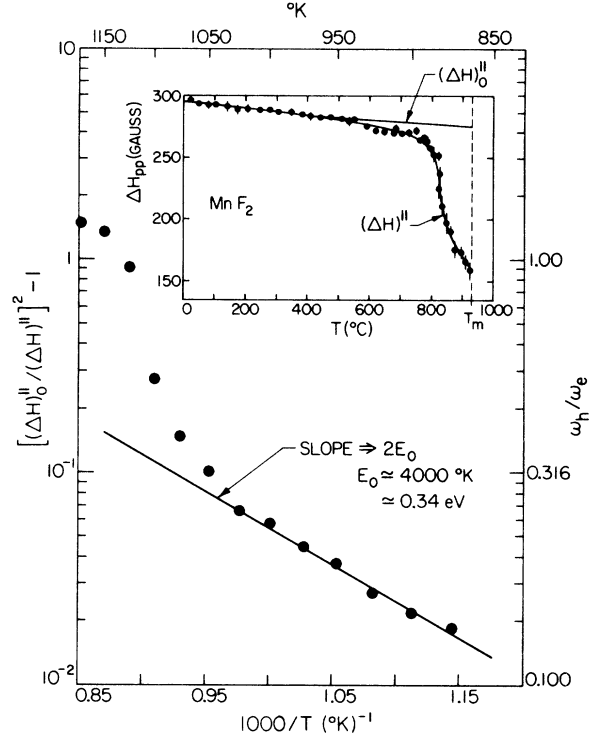


FIG. 12. Analysis of the high-temperature EPR linewidth in MnF_2 below the melting point. The inset shows $\Delta H^{\parallel}(\vec{H}_0 \parallel \vec{c})$ as taken from Fig. 4, with $(\Delta H)_0^{\parallel}$ being the extrapolated linewidth behavior, if only spin dynamical effects were present. The semilog plot of $[(\Delta H)_0^{\parallel} / \Delta H^{\parallel}]^2 - 1$ vs $1/T$ reveals thermally activated *interchange* of nearest-neighbor Mn ions [see Eq. (4.16)] with an initial slope corresponding to an activation energy of $E_0 \approx 4000 \text{ K}$.

correlations between the interchange and exchange processes for neighboring pairs of spins must become important, (ii) at the temperature where there is noticeable deviation of the data from the predictions of Eq. (4.14) ω_h has reached a value only some 30 times smaller than ω_a , and (iii) the large anharmonic content to the lattice vibrations as $T \rightarrow T_m$ would certainly contribute to a lowering of the barrier for the interchange and a temperature dependence to the attempt frequency.

Finally, the very fact that no sizable change, if any, occurs in ΔH in passing through the melting point suggests that the character of the spin dynamical motion immediately below T_m cannot differ appreciably, on a local scale, from that just above T_m .

B. Discussion of the magnetically diluted systems—solid state

1. Concentration dependence of the width and profile of the EPR

Figure 6 shows the variation of the peak-to-peak derivative width ΔH_{pp} as a function of the Mn con-

centration x in the system $\text{KMn}_x\text{Mg}_{1-x}\text{F}_3$ at 300 °K. Within the region of experimental observation (± 3 linewidths), the line profiles appear to be Lorentzian in shape for $1.0 \geq x > 0.4$. For this concentration range one might hope to extract the qualitative dependence of ΔH on x from an analysis of the second and fourth moments, M_2 and M_4 , of the line profile. An analysis of the dilution problem, in the absence of exchange narrowing, as it affects M_2 and M_4 , has been previously given.⁴⁸ Its extension to include exchange effects is straightforward.²³ One finds $M_2(x) = xM_2(1)$. However, M_4 has terms both linear and quadratic in x , as in the purely dipolar case.⁴⁸ We find that the terms linear in x are almost an order of magnitude smaller than those proportional to x^2 for $x=1$. Thus it is a good approximation to take $M_4(x) \approx x^2M_4(1)$, at least in the large- x region.

If one then approximates^{23,49} the line profile by a truncated Lorentzian or Gaussian Lorentzian shape, either of which is a two parameter function, then it immediately follows that

$$\Delta H(x) = c \frac{M_2^{3/2}}{M_4^{1/2}} = cx^{1/2} \frac{[M_2(1)]^{3/2}}{[M_4(1)]^{1/2}} \quad (4.17a)$$

or

$$\Delta H(x) = x^{1/2} \Delta H(1), \quad (4.17b)$$

where c is a constant of order unity and differs slightly for the two profiles. The solid line in Fig. 6 is a plot of Eq. (4.17b) and the experimental data measurably deviate from the predicted behavior at $x \leq 0.8$.

That the approximation of taking $M_4(x) \approx x^2M_4(1)$ is reasonable may be seen somewhat more directly from the alternate description of the linewidth as

$$\Delta \bar{H} \propto M_2 \omega_e^{-1}, \quad (4.17c)$$

where $\omega_e^2 = \frac{2}{3} \hbar^{-2} z J^2 S(S+1)$. Since $\omega_e \propto z^{1/2}$ and $\bar{z}(x) = xz(1)$, it follows that $\Delta H(x) = x^{1/2} \Delta H(1)$, as before. Now ω_e appears as the quantity which characterizes the initial Gaussian decay of the two-spin correlation function. Hence the fact that $\omega_e(x) = x^{1/2} \omega_e(1)$ implies that the decay of $\langle S_i(t) S_i(0) \rangle$ remains Gaussian, at least for small t . To the extent that a departure from purely Gaussian behavior will occur in a disordered paramagnet with increasing dilution, one may expect the linewidth to differ from the simple $x^{1/2}$ prediction. Calculations have been made⁵⁰ of the frequency moments of the two-spin correlation functions for a disordered paramagnet but no results have been obtained, as yet, for the four-spin correlation functions which would be needed to interpret the EPR.

Let us first point out that hyperfine interactions (Mn^{55} and/or F^{19}) are not the source of this discrepancy. While it is apparent that resolved hfs

is present at the lowest concentrations studied (see Fig. 5) this structure disappears above $x \approx 0.1$. The mechanism which broadens the line so as to make the structure unresolved is not the dynamic hyperfine interaction itself, but is rather the electronic dipolar interaction. This follows from a comparison of the second moment contributions of the two: $M_2^{\text{dip}}(x) = xM_2^{\text{dip}}(1)$, whereas $M_2^{\text{hfs}} = \frac{1}{3} A^2 I(I+1)$ and suffers no dilution effects. From Ref. 49 $M_2^{\text{dip}}(1) \approx 3 \times 10^{21} \text{ sec}^{-2}$ and $M_2^{\text{hfs}} \approx 3 \times 10^{19} \text{ sec}^{-2}$. Therefore in the whole of the concentration range of Fig. 6 ($1 \geq x \geq 0.2$) dipolar interactions are overwhelmingly dominant.

How then can we explain the observed behavior? One possibility is suggested by the detailed study^{23,49} of the line profiles of the EPR and NMR in the case of the pure crystals. In the perfect crystal (e.g., KMnF_3), using only M_2 and M_4 and either of the aforementioned two-parameter line profiles results in an error of at least a factor of 2 for the infinite temperature linewidth (see Table III), despite the precise knowledge of all the interaction and lattice parameters. Only by inclusion of the sixth moment M_6 and use of three-parameter line profiles that were more elaborate (truncated double Lorentzian or Gaussian double Lorentzian) could approximate agreement between the moment method analysis and experiment be achieved (see Table III). The reasons are clear; the lower-or-

TABLE III. Linewidths, predicted and observed, for the EPR of KMnF_3 extrapolated to the infinite-temperature limit. Those obtained from moment calculations assume the line profiles as indicated. The self-consistent effective-field theory result is obtained from Eq. (A18). The value computed for the Green's-function theory is obtained from our Eq. (A21). Both experimental values were obtained by taking the 400 °K values and extrapolating them to $T = \infty$ using the Green's-function theory. By so doing we utilize the low-temperature values of the dipolar and exchange constants in all calculations.

Theoretical line	Linewidth (G)
Truncated Lorentzian ^a	22
Gaussian Lorentzian ^a	30
Truncated double Lorentzian ^a	69
Gaussian double Lorentzian ^a	52
Self-consistent-effect field ^b	39
Green's function ^c	48
Sum-rule moment expansion ^d	70
Experimental results	
Gulley <i>et al.</i> ^a	64
This work	59

^a Reference 49.

^b This work.

^c Reference 9.

^d P. A. Fedders, Phys. Rev. B **3**, 2352 (1971).

der moments give information about the short-time behavior of the correlation functions. One has to go to higher and higher moments to find the long-time behavior. Thus the lower-order moments give an accurate description of the line far out in the wings, which is of minimal interest if one is trying to characterize the profile in terms of its width.

One can then recognize the limitation of the moment analysis for the dilution problem. Clearly the ratios of the higher to lower moments [e.g., $M_4/(M_2)^2$ and $M_6/(M_2)^3$] are *not* independent of x , as is implicit in the $x^{1/2}$ prediction for the variation of ΔH with x . The line must actually change shape almost immediately with increasing dilution. Of course, in the region around the line center it continues to look Lorentzian, but weight must be redistributed between the wings and central portion. We should not be surprised by this conclusion, since we know that in the purely dipolar case⁴⁸ the low-order moments already show a slow transition from roughly Gaussian ($x \gg 0.1$) to Lorentzian ($x \ll 0.1$) shape with increasing dilution. Even this case has not been analyzed completely in terms of higher-order moments, and our problem (dipolar plus exchange) is still more intractable.

There is a more microscopic approach, which is suggestive as to where the specific difficulty with regard to the observed departure from the $x^{1/2}$ behavior might occur and, in particular, why the linewidth actually increases with decreasing x below $x \approx 0.5$. In the sc lattice ($z = 6$) the number of Mn ions that have *no* Mn nn rises from 1.6% at $x = 0.5$ to 53% at $x = 0.1$. Because these isolated Mn ions are coupled to other Mn spins only by dipolar, rather than exchange, interactions, their fluctuation power spectrum is concentrated at low frequencies. Similarly the fluctuation spectra associated with a small isolated cluster of Mn spins are concentrated around a few discrete frequencies (separated by about J/n , where n is the number of spins in the cluster), always including $\omega = 0$. If two spins, S_1 and S_2 , belong to such clusters (e.g., each is an isolated spin, or the two constitute an isolated pair with no exchange interactions with other Mn spins), then the four-spin correlation function $\langle S_1(t)S_2(t)S_1(0)S_2(0) \rangle$ will decay in a time characterized by a dipole coupling; it will thus make an anomalously large contribution to the resonance width. The importance of these isolated ions (or small clusters) is not given proper attention in an approach, such as the moment calculation discussed above, where the environment of a given spin is treated only on the average.

As a crude approximation one might take the line profile to be made up of two contributions, one arising from spins within large (or the "infinite") connected clusters and the other from exchange

isolated spins or those in small clusters. Since all resonate at $g = 2$, one studies the behavior of the total transverse magnetization, and we might represent the linewidth approximately as

$$\Delta \bar{H}(x) \approx x^{1/2} \Delta H(1) + F(x)(\Delta H)_{\text{isol}}, \quad (4.18)$$

with $F(x)$ being a function related to the probability of finding isolated ions (and small clusters). There is an additional feature to the dilution experiments which is in accord with such an interpretation. As was mentioned earlier, the approximately constant slope of $\Delta H(T)$ varied as a function of x (see Table I). We may generalize (4.18) to include the approximate temperature dependence above $T = 400$ K:

$$\Delta \bar{H}(x; T) = [1 + \alpha(T - 400)]x^{1/2} \Delta \bar{H}(1; 400) + \Delta H'(x), \quad (4.19)$$

where $\Delta H'(x)$ represents the isolated cluster contribution, independent of temperature in a first approximation. The quantity α describes the variation of the linewidth arising from the anharmonic and harmonic contributions and for simplicity we assume α to be a function neither of T nor of x . Then

$$\frac{\delta \Delta \bar{H}}{\delta T} = \Delta H_0(1; 400)x^{1/2}\alpha,$$

and for large x , where $\Delta H'(x)$ is very small,

$$\frac{1}{\Delta H(x; 400)} \frac{\delta \Delta \bar{H}}{\delta T} = \alpha = \text{const.} \quad (4.20)$$

We see in Table I that this prediction is borne out and that the deviations from Eq. (4.20) at smaller x occur because the temperature independent contribution to $\Delta \bar{H}(x, T)$ from $\Delta H'(x)$ becomes increasingly important.

2. Temperature dependence of the ^{55}Mn and ^{19}F hfs

In the very low concentrations of Mn in KMgF_3 and KZnF_3 ($x \leq 10^{-3}$) both well-resolved ^{55}Mn and ^{19}F hfs appear, and their temperature dependence was studied (see Fig. 7). The magnitude and sign of the temperature-dependent ^{55}Mn hfs have been investigated in a number of substances beginning with the work of Walsh *et al.*⁵¹ Its origin was explained by Simanek and Orbach⁵² in terms of the admixture of Mn $3d^4ns$ configurations into the ground state $3d^5$ one via the orbit-lattice interaction, as driven by the *harmonic* vibrations of the crystal. The anharmonic contribution actually causes the negative hfs to increase, rather than decrease, in magnitude with increasing temperature.⁵¹ Although our measurements extend to higher temperatures than the earlier ones,⁵¹ no particular new results, with regard to the ^{55}Mn hfs, are apparent.

However, the temperature dependence of the F^{19} hfs has not been as extensively studied, and no comparison has been made between the variations of the Mn^{55} and F^{19} hfs in the same crystal. The harmonic and anharmonic effects of the lattice vibrations on the F^{19} hfs may be calculated using exactly the same procedures as were employed in Sec. IVA 1, and will be published elsewhere. A related approach to the problem has been given by Shrivastava.⁵³ Suffice it to say that primarily the temperature dependence of the F^{19} hfs arises from anharmonic, rather than harmonic, phonon contributions although, as in the case of $J(T)$, in the limit $T \gg \Theta_D$, both will vary approximately linearly with T . Thus it is not surprising that we find that the relative changes of the two hfs interactions with temperature are roughly proportional; i.e., $A^{19}(T)/A^{19}(400\text{ K}) \approx KA^{55}(T)/A^{55}(400\text{ K})$, with $K \approx 5$, despite the different origins of the hfs and the different dependence on phonon excitations (i.e., harmonic versus anharmonic) to their variations with temperature.

What is somewhat more interesting is a comparison of the relative change of the F^{19} hfs with temperature with the corresponding variation of the exchange interaction $J(T)$ in the isomorphic $KMnF_3$ and $RbMnF_3$ crystals. Since the F^{19} hfs interaction is proportional to the $Mn^{2+}-F^-$ overlap integrals²⁶ and the $Mn^{2+}-F^--Mn^{2+}$ superexchange interaction is proportional to the square of these integrals,³⁴ one might expect that the relation $J(T)/J(400\text{ K}) \approx [A(T)/A(400\text{ K})]^2$ would hold. In view of the fact that there is some uncertainty in the experimental quantities and the manner in which $J(T)/J(400\text{ K})$ was determined, as well as the fact that the two measurements relate to two different crystals (i.e., $KMgF_3$ and $KMnF_3$) it is perhaps fortuitous how closely the data seem to fit the above relation, as is seen directly by a comparison of Figs. 7 and 11. (Note difference in temperature scales in the two figures.)

C. Molten state: $T > T_m$

Regarding the measurements of the linewidth at and above the melting point T_m only very qualitative conclusions may be made, at present. Here we are limited by the absence of data on the viscosity and density and, to a larger degree, knowledge of the structure of the liquid.

Let us first consider MnF_2 . We take the decrease in ΔH in MnF_2 before melting as an indication that motion must play an important role in the narrowing of ΔH above T_m . We have already asserted that this phenomenon is tied to an interchange of Mn ions along the c axis. Since MnF_2 exhibits no radical change in ΔH as T increases from just be-

low to just above T_m , we are led to believe that motion continues to determine the decay of the relevant correlation functions. In the extreme narrowing limit we might expect⁴¹

$$\Delta H = M_2^I \tau_c^I, \quad (4.21)$$

where, for an isotropic liquid,

$$M_2 \approx \frac{5}{4} (g\mu_B)^4 \hbar^2 [S(S+1)/a_0^6] z_l,$$

with a_0 characterizing the closest-approach distance for two Mn^{2+} ions and z_l being the average near-neighbor Mn-Mn coordination number. Apart from a factor of order unity it is not unreasonable to surmise that $M_2^I \approx M_2^S$. Of course, if there is a very large change in the density ρ upon melting then this result might be somewhat altered, but it is unlikely that ρ changes by as much as 15%.

With the linewidth just below T_m nearly equal to the linewidth just above, and assuming $M_2^I = M_2^S$, we see that $\tau_c^I \approx \tau_c^S \approx 10^{-12}$ sec. Whereas below T_m motion was characterized in terms of a definite lattice-related interchange mechanism, we are somewhat less certain as to the detailed nature of the motion in the liquid. One might argue that in a strongly Coulomb-correlated ionic liquid, such as molten MnF_2 , a high degree of position-position short-range order must be present, not unlike that of the solid. What was energetically possible as an interchange mechanism in the solid would then certainly not be less so in the liquid—although here we might label this as a “chemical exchange” between Mn ions. Alternatively, if the liquid is characterized by voids, of either atomic size or larger, then the translational kinetic energy of an ion (regarded as “free”) would make possible the jumping of ions from occupied sites into adjacent empty ones in times of the order of 10^{-12} sec or less.

In a distinctly different fashion, all of the $XMnF_3$ compounds show an abrupt increase in ΔH at the melting point. Since motion appeared not to play an important role in determining ΔH in the solid state, the increase in the linewidth at T_m must be regarded first as a decrease in the exchange narrowing. However, just how much the exchange has decreased at this point is not clear, because the subsequent monotonic decrease in ΔH with increasing temperature suggests that motional narrowing immediately becomes important upon melting.

Some further insight into the relative role of motional and exchange narrowing is obtained from a consideration of the mixed systems, especially with regard to the linewidth at the melting point (see Figs. 8 and 9). Decreasing the density of magnetic ions results in an initial decrease in the linewidth which varies approximately as the square root of the magnetic concentration x . Assuming the viscosity, and hence the correlation time, to be sim-

ilar for all the melts at T_m the linewidth would be given, in the presence of motional narrowing alone, by

$$\Delta H = (xM_2^I)\tau_c^I. \quad (4.22)$$

The slower observed dependence of ΔH on x suggests that exchange continues to play an important role even at T_m . The linewidth decreases more slowly with further magnetic ion dilution. This probably results from the contribution that the isotropic ^{55}Mn hyperfine structure makes to the second moment, which may no longer be neglected relative to the larger dipolar interaction, if the latter has been motionally narrowed. Since motion has no effect on the ^{55}Mn hfs broadening, there must still be an appreciable exchange narrowing to reduce the linewidth (or rather remove the structure) from an expected value of $\Delta H \approx 2IA \approx 500$ G in the concentration region $x \lesssim 10\%$. Finally at very low concentrations ($x \lesssim 0.5\%$) the few spin exchange collisions that occur are not sufficient to narrow the hfs and the resonance again begins to broaden. Unfortunately at the very lowest concentrations studied we were not able to see a resolved ^{55}Mn hfs, although we believe eventually one must appear as $x \rightarrow 0$!

Finally, in comparing the dilution experiments in the solid with those in the liquid we note that the minimum in the linewidth occurs at a smaller value of x in the liquid. From our arguments above we believe that, in the absence of ^{55}Mn and ^{19}F hfs, the linewidth in the liquid would monotonically decrease with x . That this does not occur in the solid is a consequence of the important contribution made by isolated Mn ions which experience no exchange narrowing, as we discussed previously, and which has no counterpart in the liquid.

V. CONCLUSIONS

The systematic study of the EPR linewidth as a function of temperature in but a few magnetic salts already shows a rich variety of behavior both in the solid and molten states. It is clear that phonon-induced corrections to the dipolar and exchange interactions as they affect the EPR linewidth below T_m are of prime importance in the XMnF_3 systems. However, in MnF_2 , a physical interchange of cations at a rate comparable to the spin exchange frequency becomes a significant mechanism for the narrowing of the line below the melting point.

The linewidth measurements above T_m , in the dilute as well as in the magnetically dense salts, reveal that motion and spin exchange both contribute to the narrowing of the line. More detailed interpretation of these results awaits complementary studies of the static and dynamic properties

of the molten salts (viscosity, density, paramagnetic diffuse scattering of neutrons, nuclear magnetic resonance, etc.).

ACKNOWLEDGMENTS

The skill, effort, and dedication of N. Nighman in the preparation of all of the materials used in these experiments and his advice on sample containment, reactivity, etc., are most gratefully acknowledged. A. R. King has given generously of his time in advising and assisting in nearly all experimental phases of this work. We wish to express an appreciation to J. R. D. Copley, and R. D. Hogg for permission to quote results from their unpublished work. Many profitable discussions were had with F. Borsa, J. P. Boucher, D. Hogg, A. R. King, and K. Shrivastava concerning the interpretation of the results. A. Dormann assisted in the data analysis reduction. One of us (E.D.) was supported by a Fazit-Stiftung Fellowship during his stay at UCSB. Part of this work was completed while the other two authors were on sabbatical leave in France; the support given (D.H.) by the Laboratoire de Physique des Solides, Orsay and (V.J.) by the Institut Laue-Langevin and the Laboratoire de Spectrométrie Physique, Grenoble during their stay was most appreciated as was that provided (V.J.) by a Guggenheim Memorial Foundation Fellowship. We are indebted to R. H. Silsbee for a critical review of this work. Many of his suggestions have been incorporated into the present manuscript.

APPENDIX: RIGID-LATTICE THEORIES FOR SOLID DENSE PARAMAGNETS

1. Self-consistent effective-field theory (Ref. 54)

Mori and Kawasaki⁵ first formulated the EPR linewidth problem using a method involving the time evolution of the Kubo relaxation function. We may express the components S_j^α ($\alpha = x, y, z$) of the individual spin operators S_j^α in terms of collective operators S_q^α by

$$S_q^\alpha = N^{-1/2} \sum_j S_j^\alpha e^{i\vec{q} \cdot \vec{R}_j}. \quad (A1)$$

Then the relaxation function ($S_q^\alpha(t), S_{-q}^{\alpha'}(0)$) is defined through the ordinary correlation function $\langle S_q^\alpha(t) S_{-q}^{\alpha'}(0) \rangle$ by the relation

$$(S_q^\alpha(t), S_{-q}^{\alpha'}(0)) \equiv \int_0^\beta d\lambda \langle S_q^\alpha(t - i\lambda) S_{-q}^{\alpha'}(0) \rangle, \quad (A2)$$

with $\beta = 1/kT$. If the system is magnetically isotropic, then $(S_q^\alpha(t), S_{-q}^{\alpha'}(0)) = \delta_{\alpha\alpha'} (S_q^\alpha(t), S_{-q}^\alpha(0))$. Now if the decay rate of the corresponding torque-torque relaxation function $(\dot{S}_q^\alpha(t), \dot{S}_{-q}^\alpha(0))$ is much faster than

that of $(S_q^\alpha(t), S_{-q}^\alpha(0))$, then it is a good approximation to represent the latter's time evolution as

$$(S_q^\alpha(t), S_{-q}^\alpha(0)) = (S_q^\alpha(0), S_{-q}^\alpha(0)) e^{-\Gamma_q t}, \quad (\text{A3})$$

with

$$\Gamma_q = (S_q^\alpha(0), S_{-q}^\alpha(0))^{-1} \int_0^\infty (\dot{S}_q^\alpha(t), \dot{S}_{-q}^\alpha(0)) dt. \quad (\text{A4})$$

The time-independent normalization factor is the inverse of the static wave-vector-dependent spin susceptibility:

$$\chi^\alpha(q) \equiv (S_q^\alpha(0), S_{-q}^\alpha(0)). \quad (\text{A5})$$

The EPR linewidth corresponds to the rate Γ_0 associated with the decay of the transverse uniform magnetization. The central problem is one of evaluating $\int_0^\infty (\dot{S}_0^\alpha(t), \dot{S}_0^\alpha(0)) dt$, where the time dependence of the torque, $i\hbar \dot{S}_0^\alpha(t) = [S_0^\alpha, \mathcal{H}]$, is generated by the full spin Hamiltonian:

$$\begin{aligned} \mathcal{H} = & \sum_{j,j'} J_{jj'} \vec{S}_j \cdot \vec{S}_{j'} \\ & + g^2 \mu^2 R_{jj'}^{-5} [(\vec{S}_j \cdot \vec{S}_{j'}) R_{jj'}^2 \\ & - 3(\vec{R}_{jj'} \cdot \vec{S}_j)(\vec{R}_{jj'} \cdot \vec{S}_{j'})], \end{aligned} \quad (\text{A6})$$

in which, for Mn^{2+} salts where single-ion anisotropy is so much smaller than the interion dipolar interactions, we retain only the latter. The recognition of this fact by Huber⁷ was an important contribution relative to the original work of Mori and Kawasaki, in which only single-ion anisotropy was considered. While \mathcal{H}_{ex} commutes with S_0^α , the dipolar interaction does not. Therefore $[S_0^\alpha, \mathcal{H}_{\text{dip}}]$ will contain products of single-spin operators and hence the uniform torque relaxation function will involve products of *pairs* of single-spin operators; i.e., $(\dot{S}_0^\alpha(t), \dot{S}_0^\alpha(0))$ will contain terms of the form $(S_q^\alpha(t) S_{q'}^\alpha(t), S_{q''}^\alpha(0) S_{q'''}^\alpha(0))$. In the spirit of the random-phase approximation this may be decoupled into products of two-spin relaxation functions

$$(S_q(t) S_{q'}(t), S_{q''}(0) S_{q'''}(0)) \approx kT (S_q(t), S_{-q}(0))^2 \delta_{q'', -q}. \quad (\text{A7})$$

Following Huber⁷ then, we may express the linewidth $\Gamma_0 = 1/T_2$ as

$$\frac{1}{T_2} \approx \frac{kT}{\hbar^2 \chi(0)} \frac{1}{N} \sum_{\vec{q}} \bar{D}(\vec{q}) \int_0^\infty (S_q^\alpha(t), S_{-q}^\alpha(0))^2 dt, \quad (\text{A8})$$

with

$$\bar{D}(\vec{q}) = (U_{xx} - U_{yy})^2 + 4U_{xy}^2 + U_{xz}^2 + U_{yz}^2, \quad (\text{A9a})$$

where

$$U_{\alpha\alpha'}(\vec{q}) = \sum_j e^{i\vec{q} \cdot \vec{R}_j} (3R_{j\alpha} R_{j\alpha'} - \delta_{\alpha\alpha'} R_j^2) R_j^{-5}, \quad (\text{A9b})$$

and $\chi(0)$ is the exchange-enhanced uniform spin susceptibility.

The problem lies in the evaluation of the quantities $(S_q^\alpha(t), S_{-q}^\alpha(0))$. Up to now the main interest⁵⁻⁷ has been in the critical behavior of the linewidth near $T = T_c$. Here, instead, our primary concern is with higher temperatures: $(T - T_c)/T_c > 1$. Using Eqs. (A3) and (A5) we may write Eq. (A8) in the form

$$\begin{aligned} \frac{1}{T_2} = & \frac{g^4 \mu_B^4}{kT \chi(0)} \left(\frac{S(S+1)}{3\hbar} \right)^2 \\ & \times \frac{1}{N} \sum_{\vec{q}} \bar{D}(\vec{q}) \left(\frac{\chi(\vec{q})}{\chi_0} \right)^2 (2\Gamma_q)^{-1}, \end{aligned} \quad (\text{A10})$$

where χ_0 is the "bare" susceptibility: $\chi_0 = S(S+1)/3kT$. If one makes the reasonable assumption that the torque-torque relaxation function is characterized by a simple Gaussian decay

$$(\dot{S}_q^\alpha(t), \dot{S}_{-q}^\alpha(0)) = (\dot{S}_q^\alpha(0), \dot{S}_{-q}^\alpha(0)) e^{-t^2/\tau_q^2}, \quad (\text{A11})$$

then Γ_q may be expressed as

$$\Gamma_q = \left(\frac{\pi^{1/2} \tau_q k T \hbar^{-2}}{\chi(q)} \right) \frac{1}{N} \sum_{\vec{k}} [J(\vec{k}) - J(\vec{k} + \vec{q})] \chi(\vec{k}), \quad (\text{A12})$$

with $J(\vec{k})$ the wave-vector transform of the exchange interaction. The important point is that τ_q is neither strongly \vec{q} nor temperature dependent⁵⁵ in the temperature region of interest, $(T - T_c)/T_c > 1$; it is set by the fundamental exchange interaction strength. As its value, we take the high-temperature small- q result from an explicit direct calculation⁵⁶ of the second time derivative of Eq. (A11) at $t=0$:

$$\tau_q^{-1} \approx \omega_e \equiv [8\xi z J^2 S(S+1)/3\hbar^2]^{1/2}, \quad (\text{A13})$$

where $\xi \approx 1$. Equation (A10) is then reduced to the evaluation of static \vec{q} -dependent summations. The simplest approach, the mean-field approximation, exhibits a well-known inconsistency associated with its intrinsic neglect of short-range correlations. This can be remedied by using the Green's-function random-phase approximation.⁵⁷ An equivalent formulation⁵⁸ is the reaction field correction to the mean-field result to $\chi(q)$, which gives

$$\frac{\chi(\vec{q})}{\chi_0} = \frac{T/T_c^0}{s - J(\vec{q})/J(\vec{K}_0)}, \quad (\text{A14})$$

where \vec{K}_0 identifies the wave vector for which $\chi(\vec{q})$ diverges at $T = T_c$ and $T_c^0 = J(\vec{K}_0) S(S+1)/3k$. The parameter s and the temperature T are implicitly related by the requirement

$$\frac{1}{N} \sum_{\vec{q}} \frac{\chi(q)}{\chi_0} = 1$$

or

$$(T/T_c^0)G(s) = 1, \quad (\text{A15})$$

where

$$G(s) \equiv (2\pi)^{-3} \int d\vec{q} \left(s - \frac{J(\vec{q})}{J(\vec{K}_0)} \right)^{-1}, \quad (\text{A16})$$

the lattice Green's function, has been numerically tabulated⁵⁹ for the sc, bcc, and fcc lattices with only nearest-neighbor interactions. This approach gives the same result as does the spherical model for $\chi(\vec{q})$. At sufficiently low temperatures, where the correlation length grows substantially larger than the near-neighbor distance, this approximation, which includes only the near-neighbor correlations, must break down. In fact, the critical exponent for $\chi(\vec{K}_0)$ is given incorrectly ($\gamma = 2$ instead of $\frac{4}{3}$), but the approach should be satisfactory in the higher-temperature region in which we are primarily interested. Using Eqs. (A12), (A14), and (A16) we may finally express the linewidth, Eq. (A10) in the form

$$\begin{aligned} \frac{1}{T_2} &= \frac{C}{kT\chi(0)} [sG^2(s) - G(s)]^{-1} \\ &\times \frac{1}{N} \sum_{\vec{q}} \bar{D}(\vec{q}) \left(s - \frac{J(\vec{q})}{J(\vec{K}_0)} \right)^{-3} \left(1 - \frac{J(\vec{q})}{J(\vec{0})} \right)^{-1}, \end{aligned} \quad (\text{A17})$$

with

$$C = (\pi^{1/2} \hbar^2 \omega_e)^{-1} [\frac{1}{3} S(S+1)]^2 g^4 \mu_B^4.$$

In the limit $T \rightarrow \infty$, $sG(s)$ approaches unity and

$$\begin{aligned} \left(\frac{1}{T_2} \right)_{T \rightarrow \infty} &= \pi^{1/2} \frac{S(S+1)}{3\omega_e \hbar^2} g^4 \mu_B^4 \\ &\times \frac{1}{N} \sum_{\vec{q}} \bar{D}(\vec{q}) \left(1 - \frac{J(\vec{q})}{J(\vec{0})} \right)^{-1}. \end{aligned} \quad (\text{A18})$$

With use of the Cohen-Keffler dipolar sums,⁶⁰ Eq. (A18) may be compared directly with the infinite-temperature moment-method analysis,⁴⁹ as shown in Table III. Other theoretical calculations of $1/T_2$ are also given in the table.

As has been emphasized by Huber,⁷ the question as to whether or not $1/T_2$ diverges as $T \rightarrow T_c$ is directly related to $\bar{D}(\vec{K}_0)$. Since, by definition, $\chi(\vec{K}_0)$ diverges as $T \rightarrow T_c$ [more precisely, $\chi(\vec{K}_0 + \vec{q}, T_c) \sim q^{-2}$], a nonzero value for $\bar{D}(\vec{K}_0)$ is both necessary and sufficient for the linewidth likewise to diverge. However, our theory suggests that for those lattices for which $\bar{D}(\vec{K}_0) = 0$ an interesting "antidivergence" will occur which is related to the sum rule

$$\frac{1}{N} \sum_{\vec{q}} \frac{\chi(\vec{q})}{\chi_0} = 1.$$

If $\bar{D}(\vec{K}_0) = 0$ and $\bar{D}(\vec{q})$ is continuous for q in the neighborhood of K_0 , then those components of $\chi(\vec{q})$ which are very large near T_c are *not* contributing to $1/T_2$. As a consequence of the sum rule the remaining $\chi(\vec{q})$ for which $\bar{D}(\vec{q})$ may or may not vanish are reduced in magnitude and hence make proportionately *less* contribution to the linewidth than they would have had there been no divergence. The theory predicts that the linewidth will actually decrease as $T \rightarrow T_c$, as is observed for RbMnF₃.

In Fig. 10 we show the temperature dependence of $(1/T_2)_T / (1/T_2)_\infty$ for the sc lattice. In the limit $T_c/T \ll 1$, one may retain only the leading term in the high-temperature expansion of the linewidth in powers of J/kT . We find then

$$\begin{aligned} \left(\frac{1}{T_2} \right) / \left(\frac{1}{T_2} \right)_\infty &\approx 1 - \frac{2}{s} + \frac{3}{s} \frac{\sum \bar{D}(\vec{q})}{\sum \bar{D}(\vec{q}) [1 - J(\vec{q})/J(\vec{0})]^{-1}} \\ &\approx 1 - 0.49(T_c^0/T). \end{aligned} \quad (\text{A19})$$

Equation (A19) is also shown in Fig. 10 for purposes of comparison both with the complete theory and with the results to be given on the Green's-function theory immediately following.

2. Dynamical Green's-function theory

We recall that the exponential-decay approximation of Eq. (A3) relies on the assumed rapid decay of the corresponding torque correlation function $T_q(t) \equiv (S_q(t), S_{-q}(0))$ relative to the time scale set by $1/\Gamma_q$. Effectively $T_q(t)$ has been replaced by a δ function, of weight $\int_0^\infty d\tau T_q(\tau)$. Whereas this can readily be justified for small values of q , since $\Gamma_q \propto q^2$, it is not appropriate for large values of q , where Γ_q is of order ω_e , or the decay rate of $T_q(t)$ itself. Under the latter circumstances one expects a more Gaussian than exponential behavior for the spin relaxation function. In fact, a high-temperature moment analysis⁴⁶ of the dynamical susceptibility $\chi(\vec{q}, \omega)$, the Fourier transform of $(S_q(t), S_{-q}(0))$, demonstrates that it is Lorentzian-like at small q and more nearly Gaussian at large q .

Tomita and Tanaka⁸⁻¹⁰ have avoided this difficulty by taking an alternate approach to the calculation of the line shape, which does not make use of the perturbation expansion inherent in the Kubo-Tomita theory. Instead they examine directly the equation of motion of the two-spin Green's function whose Fourier transform is $\chi(\vec{q}, \omega)$, with all dynamics governed by the *full* Hamiltonian, including dipolar interactions. Inevitably, this generates an infinite hierarchy of equations involving successively higher-order Green's functions. The principal approximation is correlational rather than perturbational in na-

ture, with some high-order Green's function factorized so as to truncate the sequence of equations of motion. First, those equations are written for suitably defined cumulant-type Green's functions (CTGF). Then the n th-order CTGF is set equal to zero, which is essentially an n th-order random-phase approximation. Algebraic complexity increases rapidly with n , and Tomita and Tanaka cut off the sequence with neglect of the fourth-order CTGF. However, they recognize that this results in an approximation for the second-order CTGF which has an artificial structure: its spectral weight consists of two narrow peaks located at nearly equal distance from the resonance frequency, the square of that distance being the second frequency moment of the second-order CTGF. It is the nature of this sort of approximation that it correctly gives lower-order moments (or the initial behavior in terms of the Green's functions) but fails to treat higher moments properly. The effect of the neglected higher-order Green's func-

tions would be to spread the spectral weight of the second-order CTGF in some smooth fashion about the resonance frequency with a width of the order of the square root of the second moment; i.e., of the separation of the narrow peaks found in the above approximation. (The assumption is that, as in the case of the torque correlation function of the earlier treatment, the second-order CTGF spectral weight contains no important structure.) Tomita and Tanaka take this into account by replacing the second-order CTGF calculated by the above truncation with a Gaussian of a width such as to give the correct second moment. The result for the EPR line shape is of the form

$$I(\omega) = A(\omega) / \{ [\omega - \Delta(\omega)]^2 + [\Gamma(\omega)]^2 \}.$$

Since $\Delta(\omega)$, $A(\omega)$, and $\Gamma(\omega)$ characteristically vary on the scale of exchange frequencies, the center of the line is nearly Lorentzian, with a width $\Gamma(0) = 1/T_2$ which is given approximately as

$$\frac{1}{T_2} \simeq (g\mu_B)^4 \left(\frac{S(S+1)}{3} \right)^2 \left(\frac{\pi}{2} \right)^{1/2} \frac{1}{N} \left(\frac{10}{3} \right) \sum_{\vec{q}} \frac{kT\chi(\vec{q}) \left[\frac{3}{2} U_{zz}(\vec{q}) \right]^2}{2J(0) \{ [1 - j(\vec{q})] \sum_{\vec{q}'} kT\chi(\vec{q}') j(\vec{q}') [j(\vec{q}') - j(\vec{q})] \}^{1/2}}, \quad (\text{A20})$$

where $j(\vec{q}) \equiv J(\vec{q})/J(0)$ and all other symbols have been defined above. Here we have made the replacement $\langle S_q S_{-q} \rangle \approx kT\chi(\vec{q})$ appropriate to the high-temperature region of interest to us. In the denominator we have kept only terms of order J ; in general there should be added under the square-root corrections of order D/J and D^2/J^2 , where D is a measure of the dipolar coupling strength, but these corrections are relatively very small except near $q=0$. Since the summand diverges only as q^{-1} , phase-space factors minimize the importance of the small- q region and these corrections would add no appreciable contribution to the calculated linewidth. The calculation of Refs. 8 and 9 includes only the secular part of the dipolar interaction. We have multiplied the result by $\frac{10}{3}$ to account for the contribution of the nonsecular terms, which must be included for the exchange-narrowed line. The essential correctness of this procedure was demonstrated by Tomita and Tanaka in their second paper.⁹

Equation (A20) is of the form

$$N^{-1} \sum_{\vec{q}} \frac{a^2(\vec{q})}{b(\vec{q})}$$

and would lend itself only to numerical computation. Tomita and Tanaka argue that it should be an adequate approximation over the whole of the paramagnetic region to make the factorization

$$N^{-1} \sum_{\vec{q}} \frac{a^2(\vec{q})}{b(\vec{q})} \rightarrow \sum_{\vec{q}} a^2(\vec{q}) / \sum_{\vec{q}'} b(\vec{q}')$$

on the grounds that the distribution with respect to \vec{q} is quite different for $a^2(\vec{q})$ and $b(\vec{q})$, the former being primarily dipolar and the latter exchange in character. By so doing they are able to Fourier transform $a^2(\vec{q})$ and $b(\vec{q})$ into their configuration space counterparts, which are easily evaluated. For the sc lattice their final expression for the linewidth is [Eq. (18) of Ref. 9]

$$\frac{1}{T_2} \simeq \frac{3\sqrt{3}\pi}{16} \frac{\sum_{|\vec{\delta}|} \alpha(|\vec{\delta}|) \gamma(|\vec{\delta}|)}{|J| [\gamma(0) + \gamma(1) + 4\gamma(\sqrt{2}) + \gamma(2)]^{1/2}}, \quad (\text{A21})$$

where the $\gamma(\vec{m})$ are the static two-spin correlation functions of magnetic atoms separated by a lattice vector $\vec{m}a_0$. The quantities $\alpha(|\vec{\delta}|)$ are defined by the inverse Fourier transform of the dipolar factor $[U_{zz}(\vec{q})]^2$ in the numerator of Eq. (A20).

The result (A20) for $1/T_2$ is in a form which can be compared directly with the self-consistent effective-field-theory expression (A10) with the definition of Γ_q (A12). In both cases $1/T_2 \sim D^2/J$ at high temperatures, as expected on general grounds. However, the weighting of different regions of the Brillouin zone is quite different, leading to a substantially different temperature

dependence of T_2 relative to its infinite temperature value.

Numerical computations of $(1/T_2)_T/(1/T_2)_\infty$ were made using Eq. (A21) with the nn, nnn, and nnnn static

pair-correlation functions obtained from high-temperature expansion of the random-phase Green's-function theory for these quantities.⁵⁷ We obtain then

$$\left(\frac{1}{T_2}\right)_T / \left(\frac{1}{T_2}\right)_\infty = \frac{1 - 1.0390 T_0/T - 1.4943(T_0/T)^2 - 3.1170(T_0/T)^3}{[1 - T_0/T + 5.8612(T_0/T)^2 - 3(T_0/T)^3]^{1/2}}, \quad (\text{A22})$$

with $T_0 \equiv \frac{1}{3}JS(S+1) = 0.2528 T_N$ in the Green's-function theory for the sc lattice. The results obtained from Eq. (A22) are shown in Fig. 10 and again we have also plotted the same ratio to order T_0/T ; namely

$$\begin{aligned} (1/T_2)_T / (1/T_2)_\infty &\approx 1 - 0.54 T_0/T \\ &\approx 1 - 0.090 T_c^0/T. \end{aligned} \quad (\text{A23})$$

This leading term is seen to give most of the temperature dependence in the region $T/T_N > 5$, which is the primary region of interest for our high-temperature studies. It is also apparent that the self-consistent effective-field theory yields a larger coefficient of T_c^0/T , the two theories differing by a factor of 5.

Considering the nature of the approximations contained in the Tomita-Tanaka theory, it is not immediately apparent that its predictions are to be preferred to those obtained from our own. However, we have also compared the predictions of the self-consistent effective-field theory for the NMR problem⁵⁵—as to the temperature dependence of the auto- and pair-correlation functions—with the results of exact high-temperature expansions^{61,62} and found our theory to *overestimate*⁶³ the coefficient of T_0/T in each case. In the absence of any other detailed calculations for the EPR linewidth problem we have elected to use the Tomita-Tanaka results as “exact” for all further discussions in connection with the interpretation of the experimental results.

Apart from all other features of the Green's-function theory, what is abundantly clear from Fig. 10 is that in the region $T/T_N > 5$ the linewidth changes by no more than (2–3)% before melting ($T_m/T_N \approx 15$). Hence the observed increase of some 15% in ΔH in KMnF_3 and RbMnF_3 cannot be mainly of spin-dynamical origin.

Finally, we have collected in Table III the predictions for the infinite-temperature linewidth for KMnF_3 from moment and other theories along with the results obtained from the two theories discussed in this section to compare with the experimental results. The experimental values are the room-temperature results extrapolated to $T = \infty$ using the Tomita-Tanaka theory. In this way we

remove the observed changes in ΔH that occur at higher temperatures which we believe to be of non-spin-dynamical origin.

In this section we have shown that a relatively simple theory of the spin dynamics as it relates to the EPR linewidth problem gives qualitatively good results as to the absolute magnitude of ΔH and its temperature dependence. A more elaborate theory, that of Tomita-Tanaka, shows the temperature dependence of ΔH to be even weaker at high temperatures and hence we conclude the *observed* results cannot arise primarily from “rigid-lattice” spin-dynamical effects.

In the interpretation we have employed a theory of the spin dynamics involving several approximations whose validity is difficult to assess with confidence. We know, as pointed out above, that the approximate static correlation functions used are inaccurate in the critical region; the critical exponents are incorrect. But even well above this region, in the intermediate temperature range $2 < T/T_N < 5$, where short-range-order effects lead to considerable temperature variation of the predicted linewidth (Fig. 10), there is substantial disagreement with experiment (ΔH nearly temperature independent; Fig. 3). Why have we then accepted the theory as reasonable at higher temperatures? The answer is that we believe a major source of the discrepancy in the intermediate temperature range to be a gradual change of the line shape with temperature, as evidenced clearly in the theoretical work of Mori⁶⁴ at temperatures closer to the critical point. The problem is that a single parameter characterizing the line, the linewidth ΔH , has been estimated by calculation of a few low-order moments determining the short-time behavior of the correlation functions. But we know⁴⁹ that the connection between these moments and ΔH is sensitive to the precise nature of the cutoff of the wings of the assumed line shape, known to be Lorentzian near its center; the difference can be as much as a factor of two in predicted linewidth for different reasonable decays in the distant wings of the line. We do not, however, expect the line shape to change appreciably in the high-temperature region, before short-range order begins to play a substantial role.

- *Research supported in part by the National Science Foundation.
- †Present address: Institut II für Festkörperphysik, Technische Hochschule, 61 Darmstadt, Hochschulstrasse 2, West Germany.
- ¹L. Yarmus, M. Kukk, and B. R. Sundheim, *J. Chem. Phys.* **40**, 33 (1964).
 - ²T. B. Swanson, *J. Chem. Phys.* **45**, 179 (1966).
 - ³B. R. Sundheim, J. Flato, and L. Yarmus, *J. Chem. Phys.* **51**, 4132 (1969).
 - ⁴R. D. Hogg, Ph.D. thesis (UCSB, 1975) (unpublished).
 - ⁵H. Mori and K. Kawasaki, *Prog. Theor. Phys.* **27**, 529 (1962).
 - ⁶H. Mori, *Prog. Theor. Phys.* **34**, 399 (1965).
 - ⁷D. L. Huber, *J. Phys. Chem. Solids* **32**, 2145 (1971); *Phys. Rev. B* **6**, 3180 (1972).
 - ⁸K. Tomita and M. Tanaka, *Prog. Theor. Phys.* **29**, 528 (1963).
 - ⁹M. Tanaka and K. Tomita, *Prog. Theor. Phys.* **29**, 651 (1963).
 - ¹⁰K. Tomita and M. Tanaka, *Prog. Theor. Phys.* **33**, 1 (1965).
 - ¹¹R. D. Hogg, *Rev. Sci. Instrum.* **44**, 582 (1973).
 - ¹²L. S. Singer, W. H. Smith, and G. Wagoner, *Rev. Sci. Instrum.* **32**, 213 (1961).
 - ¹³"Boralloy," Union Carbide Co.
 - ¹⁴The values of ΔH_{pp} (for Lorentzian line profiles) that are given throughout this work represent an average of ΔH that was determined in two ways: (i) from the field separation of the derivative extrema, and (ii) by taking half the field separation between those points in the wings of the line where the slope decreased to 0.653 of its maximum value. For the ideal Lorentzian line these two quantities are identical. Differences that were observed in these two measurements as well as the uncertainties that arise from signal-to-noise considerations, etc., constitute the origin of the error bars indicated in all plots. Field calibration was achieved with a Varian F-8 proton NMR fluxmeter combined with precision frequency measurements with a Hewlett-Packard counter.
 - ¹⁵M. S. Seehra, *Rev. Sci. Instrum.* **39**, 1044 (1968).
 - ¹⁶C. P. Poole, *Electron Spin Resonance* (Wiley, New York, 1967).
 - ¹⁷M. Peter, D. Shaltiel, J. H. Wernick, H. J. Williams, J. B. Mock, and R. C. Sherwood, *Phys. Rev.* **126**, 1395 (1962).
 - ¹⁸R. P. Gupta and M. S. Seehra, *Phys. Lett. A* **33**, 347 (1970); E. Toyota and K. Hirakawa, *J. Phys. Soc. Jpn.* **30**, 692 (1971).
 - ¹⁹K. Horai and K. Saiki, *J. Phys. Soc. Jpn.* **21**, 397 (1966).
 - ²⁰K. Lee, A. M. Portis, and G. L. Witt, *Phys. Rev.* **132**, 144 (1963).
 - ²¹M. S. Seehra and T. G. Castner, *Solid State Commun.* **8**, 787 (1970); M. S. Seehra, *J. Appl. Phys.* **42**, 1290 (1971).
 - ²²M. S. Seehra, *Phys. Rev. B* **6**, 3186 (1972).
 - ²³J. E. Gulley, Ph.D. thesis (UCSB, 1970) (unpublished).
 - ²⁴The rf losses at lower frequencies 10–100 MHz have been studied (Ref. 4) by Hogg in the course of performing NMR measurements. At these frequencies KMnF_3 appears to be little different from MnF_2 in regard to the electrical losses at higher temperatures. R. D. Hogg (private communication).
 - ²⁵J. E. Gulley and V. Jaccarino, *Phys. Rev. B* **6**, 58 (1972).
 - ²⁶A. M. Clogston, J. P. Gordon, V. Jaccarino, M. Peter, and L. R. Walker, *Phys. Rev.* **117**, 1222 (1960).
 - ²⁷Existence of the cubic as well as a monoclinic structure for KMgF_3 is known; e.g., Sh. Ogawa and Y. Yokozawa, *J. Phys. Soc. Jpn.* **14**, 1116 (1959). Our analysis of the $\text{KMn}_x\text{Zn}_{1-x}\text{F}_3$ data indicated that the monoclinic structure, often found in this series, is correlated with nonstoichiometry; stoichiometry seems easier to obtain for components with similar melting points (KMnF_3 and KMgF_3).
 - ²⁸R. C. DeVries and R. Roy, *J. Am. Chem. Soc.* **75**, 2479 (1953).
 - ²⁹Our procedure of using a low-power Impatt diode as rf source and samples bigger than the skin depth in order to have a well-defined line shape but with the disadvantage of a considerably reduced Q of the cavity due to the conduction losses in the molten sample is clearly unfavorable for the low-concentrated samples.
 - ³⁰We used a locked klystron (≈ 200 mW), balanced mixer, first or second derivative detection, and mixed a powder sample with boron nitride to reduce conduction losses. This sample-preparation technique proved, however, much less reliable than our usual measuring procedure. The super hfs splitting was smeared somewhat after the melting cycle, showing non-negligible sample deterioration.
 - ³¹E. Dormann and V. Jaccarino, *Phys. Lett. A* **48**, 81 (1974).
 - ³²D. Bloch and R. Georges, *C. R. Acad. Sci. (Paris)* **262**, 1256 (1956).
 - ³³D. Bloch, *J. Phys. Chem. Solids* **27**, 881 (1966).
 - ³⁴K. C. Johnson and A. J. Sievers, *Phys. Rev. B* **10**, 1027 (1974).
 - ³⁵R. L. Melcher and D. I. Bolef, *Phys. Rev.* **178**, 864 (1969).
 - ³⁶J. R. D. Copley, E. Dormann, and V. Jaccarino (unpublished results) (private communication).
 - ³⁷K. N. Shrivastava and V. Jaccarino, *Phys. Rev. B* **13**, 299 (1976).
 - ³⁸N. L. Huang and R. Orbach, *Phys. Rev.* **154**, 487 (1967).
 - ³⁹N. Bloembergen, E. M. Purcell, and R. V. Pound, *Phys. Rev.* **73**, 679 (1948).
 - ⁴⁰M. Eisenstadt, *Phys. Rev.* **132**, 630 (1963); M. Eisenstadt and A. G. Redfield, *ibid.* **132**, 635 (1963).
 - ⁴¹A. Abragam, *Principles of Nuclear Magnetism* (Oxford U. P., Oxford, 1961). An extensive development and review of this subject is contained in this work as regards the NMR problem.
 - ⁴²J. P. Boucher, *Phys. Rev. B* **4**, 3819 (1971).
 - ⁴³See, for example, A. B. Lidiard, *Handbuch der Physik* (Springer, Berlin, 1957), Vol. xx.
 - ⁴⁴Mention of the interchange mechanism ("platzwechsel") is made in the classic work of J. Frenkel, *Kinetic Theory of Liquids* (Clarendon, Oxford, 1946).
 - ⁴⁵C. Trapp and J. W. Stout, *Phys. Rev. Lett.* **10**, 157 (1963).
 - ⁴⁶P. G. de Gennes, *J. Phys. Chem. Solids* **4**, 223 (1958).
 - ⁴⁷This has been inferred from the fact that the temperature dependence of the lattice constants is smaller in MnF_2 than in KMnF_3 as established by the elastic-neutron-scattering measurements (see Ref. 36).
 - ⁴⁸C. Kittel and E. Abrahams, *Phys. Rev.* **90**, 238 (1953).
 - ⁴⁹J. E. Gulley, D. Hone, B. G. Silbernagel, and D. Scalapino, *Phys. Rev. B* **1**, 1020 (1970).

- ⁵⁰R. A. Tahir-Kheli and K. Kawasaki, *Phys. Rev. B* **11**, 3413 (1975).
- ⁵¹W. M. Walsh, Jr., J. Jeener, and N. Bloembergen, *Phys. Rev.* **139**, A1338 (1965).
- ⁵²E. Simanek and R. Orbach, *Phys. Rev.* **145**, 191 (1966).
- ⁵³K. N. Shrivastava, *J. Phys. C* **2**, 777 (1969). Unfortunately, the sign of the harmonic (explicit) phonon contribution is incorrect as given here.
- ⁵⁴C. Scherer, J. E. Gulley, D. Hone, and V. Jaccarino, *Rev. Brasileira Fis.* **4**, 299 (1974). In this reference the self-consistent effective-field theory was first applied to the problem of NMR in the paramagnetic state.
- ⁵⁵G. F. Reiter, *Phys. Rev. B* **7**, 3325 (1973).
- ⁵⁶The value of ξ given in Ref. 5 is not quite correct; $\xi = 1 - (1/z)[1 + 3/8S(S + 1)]$, D. Hone and C. Scherer (private communication).
- ⁵⁷M. E. Lines, *Phys. Rev.* **139**, A1304 (1965).
- ⁵⁸R. Brout and H. Thomas, *Physics* **3**, 317 (1967).
- ⁵⁹T. Morita and T. Horiguchi, *Table of the Lattice Green's Function for the Cubic Lattices* (Tohoku University, Sendai, Japan, 1971).
- ⁶⁰M. H. Cohen and F. Keffer, *Phys. Rev.* **99**, 1128 (1955).
- ⁶¹T. Moriya, *Prog. Theor. Phys.* **16**, 23 (1956).
- ⁶²D. Hone and B. G. Silbernagel, *J. Phys. (Paris) Suppl.* **32**, C1-761 (1971).
- ⁶³For the case of the auto- and pair-correlation contributions to the linewidth of the NMR the prefactors to T_0/T differ approximately by the ratios $2S(S + 1)$ and z , respectively.
- ⁶⁴H. Mori, *Prog. Theor. Phys.* **30**, 578 (1963).